

Collider Signatures of Coannihilating Dark Matter in Light of the B-Physics Anomalies

Michael J. Baker,^a Darius A. Faroughy,^b Sokratis Trifinopoulos^c

^a*ARC Centre of Excellence for Dark Matter Particle Physics, School of Physics, The University of Melbourne, Victoria 3010, Australia*

^b*Physik-Institut, Universität Zürich, 8057 Zürich, Switzerland*

^c*INFN, Sezione di Trieste, SISSA, Via Bonomea 265, 34136, Trieste, Italy*

E-mail: michael.baker@unimelb.edu.au, faroughy@physik.uzh.ch, sokratis.trifinopoulos@ts.infn.it

ABSTRACT: Motivated by UV explanations of the B -physics anomalies, we study a dark sector containing a Majorana dark matter candidate and a coloured coannihilation partner, connected to the Standard Model predominantly via a U_1 vector leptoquark. A TeV scale U_1 leptoquark, which couples mostly to third generation fermions, is the only successful single-mediator description of the B -physics anomalies. After calculating the dark matter relic surface, we focus on the most promising experimental avenue: LHC searches for the coloured coannihilation partner. We find that the coloured partner hadronizes and forms meson-like bound states leading to resonant signatures at colliders reminiscent of the quarkonia decay modes in the Standard Model. By recasting existing dilepton and monojet searches we exclude coannihilation partner masses less than 280 GeV and 400 GeV, respectively. Since other existing collider searches do not significantly probe the parameter space, we propose a new dedicated search strategy for pair production of the coloured partner decaying into $bb\tau\tau$ final states and dark matter particles. This search is expected to probe the model up to dark matter masses around 600 GeV with current luminosity.

Contents

1	Introduction	1
2	Theoretical Motivation and the Simplified Model	3
2.1	General Setup	3
2.2	UV Realisation: Majorana Dark Matter in a 4321 Model	5
2.3	The Simplified Model	7
3	Dark Matter Relic Surface	8
4	Coloured Coannihilation Partner Phenomenology	11
4.1	Ψ -Meson Spectroscopy	12
4.2	Collider Signatures	13
4.2.1	Search for Psionium in the Dilepton Channel	13
4.2.2	ψ Pair Production	14
4.2.3	Single ψ Production	15
5	Dedicated Search for ψ Pairs	15
5.1	Event Selection and Key Observables	16
5.2	Multivariate Analysis	19
5.3	Results	20
6	Conclusions	21
7	Acknowledgements	23
A	4321 models	23
B	Partial Width Formulae	24
C	Bound State Formation	25
D	Production and Decay Rate of Psionium Ψ^1	25

1 Introduction

The Standard Model (SM) of particle physics is the most accurate description of the fundamental particles and their interactions. There are, however, solid experimental and theoretical reasons to postulate the existence of New Physics (NP), e.g., astrophysical observations have established the presence of dark matter in the universe [1]. Since dark

matter cannot be accounted for by the particle content of the SM, its nature remains one of the biggest mysteries in modern physics.

At the high-energy frontier, no definite Beyond the SM (BSM) signals have emerged from the full set of run-II LHC data. However, in the last decade a large number of low-energy flavour experiments performed at B -factories and LHCb have uncovered indirect hints of lepton flavour universality violation in B -mesons decays in $b \rightarrow s\ell^+\ell^-$ and $b \rightarrow c\ell^\pm\nu$ transitions. Interestingly, these deviations from the SM, known as the B -physics anomalies, seem to point towards a new boson at the TeV scale, which couples predominantly to third generation fermions. The only models that can simultaneously accommodate all B -physics anomalies while satisfying the rich low-energy phenomenology and high- p_T constraints feature leptoquarks as the mediators of the NP effects [2–16].

In particular, the vector leptoquark U_1 with SM quantum numbers $(\mathbf{3}, \mathbf{1}, 2/3)$ has emerged as the only single-mediator solution [17–19]. Within the scope of ultraviolet (UV) complete frameworks, this vector leptoquark can arise as a gauge boson of a spontaneously broken gauge group containing $SU(3)_c$ colour as a subgroup. The minimal phenomenologically viable group is $SU(4) \times SU(3)' \times SU(2)_L \times U(1)_{T_R^3}$; models based on this group are called ‘4321 models’ [20–27]. These particular UV models predict other heavy gauge bosons, e.g., a Z' and a colour octet (coloron), that give rise to a rich set of collider signatures that can currently be tested at the LHC [28, 29]. In addition, these models introduce a wide range of new fermionic states, which may also lead to new collider signatures.

Inspired by these UV constructions, we explore the possibility that dark matter is contained within a new fermionic multiplet, which would be intimately connected to QCD through a larger gauge symmetry.¹ In particular, we investigate whether dark matter could be a neutral remnant of a fermionic multiplet of the broken gauge symmetry, much in the same way leptons are colourless remnants of a multiplet unifying quarks and leptons (as in the Pati-Salam model [51]). This would suggest that there may be other dark sector fermionic partners similar in mass to the dark matter particle that carry colour and electric charge. The U_1 leptoquark and other new gauge bosons may then mediate interactions between the dark sector and the SM.

Furthermore, a Majorana mass term generated by higher-dimensional operators induces a pseudo-Dirac scenario [52] where the would-be Dirac dark matter fermion splits into two Majorana fermions, the lighter being a dark matter candidate. We show that the quasi-degeneracy of the dark matter candidate and its coloured partner can be naturally preserved within our general UV framework, and can have a significant impact on the thermal freeze-out of dark matter and collider phenomenology. For example, the relic abundance will be determined by coannihilating effects in the early universe. The coloured coannihilating partner also hadronizes and forms QCD bound states, which may lead to unexpected signatures at the LHC.

The best probe of the dark sector is LHC production of two coannihilation partners. These can either form a bound state with each other, which then decays into dileptons via

¹For other works that propose a connection between the B -physics anomalies and dark matter, see refs. [30–50].

electroweak interactions, or each partner can decay via a leptoquark, leading to a $b\bar{b}\tau^-\tau^+$ and missing transverse energy signature. Since the b and τ particles will be soft, due to the quasi-degeneracy of the dark sector, existing ATLAS [53, 54] and CMS [55, 56] searches are not sensitive. We propose a dedicated search in this channel which exploits a novel observable: the ratio between the visible and missing energy of the process. By simulating signal and background events, we estimate the reach at the LHC (with run-II luminosity) of both a cut-based and a multi-variate analysis, finding a significant improvement when using a boosted decision tree (BDT) classifier.

The paper is structured as follows. In section 2 we first motivate the simplified model from a UV perspective, and then present the Lagrangian relevant at the TeV scale. The coannihilation effects are described in section 3 and the parameters required to reproduce the observed dark matter relic abundance are calculated. In section 4 we describe the hadronization of the coannihilating partner and the resulting meson spectroscopy. We then examine the main experimental constraints set by existing collider searches and derive bounds on the relevant parameter space. Finally, in section 5, we present our dedicated search strategy for the pair production of the coannihilating partner.

2 Theoretical Motivation and the Simplified Model

Although we will study a simplified model, we first motivate Majorana dark matter coannihilating with a slightly heavier colour triplet partner from a UV perspective. Under the SM group $SU(3)_c \times SU(2)_L \times U(1)_Y$ the dark sector states will have the representations

$$\chi \sim (\mathbf{1}, \mathbf{1}, 0), \quad \psi \sim (\mathbf{3}, \mathbf{1}, 2/3), \quad (2.1)$$

and couple directly to the vector leptoquark $U_1 \sim (\mathbf{3}, \mathbf{1}, 2/3)$. There are two main ways of accounting for a multi-TeV vector leptoquark: gauge models and strongly interacting models [28]. In this work we will assume a gauge model explanation, where the leptoquark is a massive gauge boson associated with the spontaneous breaking of a gauge symmetry, $G_{\text{NP}} \supset G_{\text{SM}}$.

2.1 General Setup

We assume that in addition to the SM matter content, there is also a heavy vector-like fermion transforming under some representation of G_{NP} that decomposes as

$$\mathcal{X} = \chi \oplus \psi \oplus \dots \quad (2.2)$$

under the SM gauge group. Although the simplest example is to take $\mathcal{X} = (\psi^1 \psi^2 \psi^3 \chi)^T$ transforming as the fundamental of $SU(4)$, we emphasise that the setup is more general and eq. (2.2) is strictly all that is required. After the breaking of G_{NP} , ψ becomes coloured under $SU(3)_c$ and χ remains colourless and electrically neutral, with quantum numbers given by eq. (2.1). We imagine that \mathcal{X} is charged under some stabilising symmetry while the SM particles are not, so the components of \mathcal{X} constitute a dark sector and the neutral component leads to a dark matter candidate. The breaking of $G_{\text{NP}} \rightarrow G_{\text{SM}}$ around the

TeV scale typically requires a set of scalar fields uncharged under the stabilising symmetry that we denote collectively as Ω . Since \mathcal{X} is a Dirac field by construction, we introduce non-renormalizable interactions so that the neutral component χ gives rise to Majorana dark matter.² This then points towards a higher scale (beyond the TeV) associated with fermion number violation.

Before the spontaneous symmetry breaking of G_{NP} , the effective Lagrangian for the dark sector up to dimension $d=5$ is

$$\mathcal{L}_{\text{eff}}^{\text{DS}} = i\bar{\mathcal{X}}\not{D}\mathcal{X} - m_{\mathcal{X}}\bar{\mathcal{X}}\mathcal{X} - \sum_n \frac{c_n^{(5)}}{\Lambda} \mathcal{O}_n^{(5)}, \quad (2.3)$$

where Λ is a large cut-off scale associated with fermion number violation and $\mathcal{O}_n^{(5)}$ are effective operators with Wilson coefficients $c_n^{(5)}$. Since \mathcal{X} is a vector-like fermion, the operators $\mathcal{O}_n^{(5)}$ fall into two possible categories: (i) operators of the form $\bar{\mathcal{X}}F\mathcal{X}$ that conserve fermion number, and (ii) Weinberg type operators of the form $\bar{\mathcal{X}}^c F'\mathcal{X}$ that violate fermion number by two units. Here F and F' are $d=2$ scalar operators that are bilinears in the fields Ω responsible for spontaneous symmetry breaking. Once these scalar fields develop vacuum expectation values (vevs) the $\mathcal{O}_n^{(5)}$ terms in eq. (2.3) will lead to both Dirac and Majorana masses for the components of \mathcal{X} of the form $\langle F \rangle / \Lambda$ and $\langle F' \rangle / \Lambda$, respectively. These masses will be suppressed because the scale Λ associated with fermion number violation is taken to be much larger than the G_{NP} breaking scale. In fact, we will assume that $\Lambda^2 \gg \langle F \rangle, \langle F' \rangle, m_{\mathcal{X}}^2$. In section 2.2 we provide a simple 4321 extension that gives rise to these two types of $d=5$ effective operators.

Note that the Lagrangian eq. (2.3) is not completely general since there could also be $d=4$ Yukawa terms of the form $\bar{\mathcal{X}}\Omega\mathcal{X}$, if the scalar sector Ω contains states with the correct quantum numbers (e.g., the adjoint scalar Ω_{15} in the 4321 model discussed in appendix A). Once these fields acquire vevs, $\bar{\mathcal{X}}\Omega\mathcal{X}$ could lead to a mass splitting of order $\langle \Omega \rangle$ between the ψ and χ components of the \mathcal{X} multiplet, while still preserving colour. We here assume that these type of $d=4$ terms are not present or are negligible (e.g., due to small Yukawa couplings) and that the only relevant sources of mass-splitting at tree level between the \mathcal{X} components arise from $d=5$ operators or higher. Higher order effective operators with $d \geq 6$ can also be included in eq. (2.3), but these will have little impact on the dark sector phenomenology and for this reason can be dropped.

After the breaking of G_{NP} , the scenario described above will lead to the following mass terms for the dark sector particles:

$$\mathcal{L}_{\text{mass}}^{\text{DS}} = -m_{\psi}\bar{\psi}\psi - m_{\chi}\bar{\chi}\chi - \frac{1}{2} (m_L \bar{\chi}_L^c \chi_L + m_R \bar{\chi}_R^c \chi_R + \text{h.c.}), \quad (2.4)$$

²Although the field content in our setup is similar to that considered in ref. [44], the dark matter candidate in ref. [44] is a Dirac fermion. For Dirac dark matter, the dominant interaction that connects the dark and SM sectors is via a Z' gauge boson and the strongest experimental limits come from direct detection experiments. Once appropriate non-renormalizable operators are included, the dark matter candidate becomes a Majorana fermion, the dominant interaction is mediated by a U_1 vector leptoquark and direct detection constraints are negligible. Instead, collider searches are the best probes of the motivated parameter space.

where m_ψ and m_χ are two Dirac masses roughly of the same order, satisfying $m_\psi = m_\chi$ and $|m_\psi - m_\chi| \sim \langle F \rangle / \Lambda \ll m_\chi$, and m_L and m_R are two small Majorana masses of order $\sim \langle F' \rangle / \Lambda$, such that $m_{L,R} \ll m_\chi$. Note that in general we expect $m_{L,R}^2 \lesssim \langle F' \rangle$ as the Majorana mass terms in eq. (2.4) violate the G_{NP} symmetry, so they may only break it softly at scales lower than the breaking scale. The resulting mass eigenstates $\chi_{1,2}$ are two pseudo-Dirac fermions [52, 57] with quasi-degenerate masses $m_{\chi_{1,2}}$, given by

$$\chi_1 \simeq \frac{i}{\sqrt{2}} (\chi - \chi^c), \quad m_{\chi_1} \simeq m_\chi - \frac{m_L + m_R}{2}, \quad (2.5)$$

$$\chi_2 \simeq \frac{1}{\sqrt{2}} (\chi + \chi^c), \quad m_{\chi_2} \simeq m_\chi + \frac{m_L + m_R}{2}, \quad (2.6)$$

up to leading order in $|m_L - m_R|/m_\chi$ and the Majorana condition $\chi_{1,2} \simeq \chi_{1,2}^c$ is satisfied up to the same order. In the mass basis, the Lagrangian reads

$$\mathcal{L}^{\text{DS}} = \bar{\psi}(i\not{D} - m_\psi)\psi + \sum_{i=1,2} \frac{1}{2} \bar{\chi}_i (i\not{D} - m_{\chi_i}) \chi_i. \quad (2.7)$$

At tree level, the spectrum of the dark sector satisfies $m_{\chi_1} \simeq m_{\chi_2} \simeq m_\psi$ with mass splittings of order $\langle F \rangle / \Lambda \sim \langle F' \rangle / \Lambda$. In what follows we will be interested in the compressed spectrum scenario $m_{\chi_1} \lesssim m_\psi \lesssim m_{\chi_2}$, so that the lightest stable state χ_1 is a dark matter candidate. Small deviations from eqs. (2.5) and (2.6) can occur at loop level if additional heavy states couple differently to ψ and χ . For example, the heavy gauge bosons in the 4321 models produce order 10% mass splittings between ψ and χ [44].

In summary, we see that relatively general considerations lead to models with a dark sector containing a coloured partner ψ and pseudo-Dirac pairs χ_1 and χ_2 , where χ_1 , χ_2 and ψ have a compressed spectrum.

2.2 UV Realisation: Majorana Dark Matter in a 4321 Model

In order to further motivate the general setup presented above, we present a concrete example of a UV model which gives rise to the dark sector effective Lagrangian eq. (2.3). For this, we extend the matter field content of the standard (or flavoured) 4321 model (see appendix A for more details) with a dark sector containing a \mathbb{Z}_2 -odd vector-like fermion $\mathcal{X} \sim (\mathbf{4}, \mathbf{1}, \mathbf{1}, +1/2)$ with components $\mathcal{X} = (\psi, \chi)^T$, and a \mathbb{Z}_2 -odd right-handed fermion singlet $S_R \sim (\mathbf{1}, \mathbf{1}, \mathbf{1}, 0)$. The role of this exact \mathbb{Z}_2 symmetry is to stabilise the dark matter. The \mathbb{Z}_2 -even SM fields are exactly as in the 4321 models, as shown in table 3. The scalar sector of 4321 contains the \mathbb{Z}_2 -even state $\Omega_1 \sim (\bar{\mathbf{4}}, \mathbf{1}, \mathbf{1}, -1/2)$, which gives rise to Yukawa interactions between the dark sector fields. The Lagrangian of the dark sector reads

$$\mathcal{L}^{\text{DS}} = \bar{\mathcal{X}}(i\not{D} - m_\mathcal{X})\mathcal{X} + i\bar{S}_R \not{\partial} S_R - \left(\frac{M_S}{2} \bar{S}_R^c S_R + \lambda \bar{S}_R^c \Omega_1^T \mathcal{X}_R + \lambda' \bar{\mathcal{X}}_L \Omega_1^* S_R + \text{h.c.} \right). \quad (2.8)$$

It is convenient to rotate the singlet fields into the Majorana basis and work with the field N defined by

$$N \equiv e^{i\frac{\theta}{2}} S_R + e^{-i\frac{\theta}{2}} S_R^c, \quad (2.9)$$

such that $N = N^c$ and where the θ phase corresponds to the argument of the Majorana mass, $M_S = |M_S| \exp(i\theta)$. We also define the couplings $\lambda_R \equiv \lambda \exp(-i\theta/2)$ and $\lambda_L \equiv \lambda' \exp(-i\theta/2)$. We can now rewrite the terms involving S_R in eq. (2.8) as

$$\begin{aligned} \mathcal{L}^{\text{DS}} \supset & \frac{1}{2} \bar{N} (i\not{\partial} - M_N) N - \frac{1}{2} \bar{N} \left[\Omega_1^T (\lambda_R \mathcal{X}_R + \lambda_L^* \mathcal{X}_L) + \Omega_1^\dagger (\lambda_R^* \mathcal{X}_R^c + \lambda_L \mathcal{X}_L^c) \right] \\ & - \frac{1}{2} \left[(\lambda_R \bar{\mathcal{X}}_R^c + \lambda_L^* \bar{\mathcal{X}}_L^c) \Omega_1 + (\lambda_R^* \bar{\mathcal{X}}_R + \lambda_L \bar{\mathcal{X}}_L) \Omega_1^* \right] N. \end{aligned} \quad (2.10)$$

The Majorana mass $M_N \equiv |M_S|$ is assumed to be much larger than the Dirac mass of \mathcal{X} , $M_N \gg m_{\mathcal{X}}$, since it is generated at a very high scale where fermion number is violated. This allows us to integrate out the N field, giving rise to the effective Lagrangian given in eq. (2.3) with the following $d = 5$ operators and corresponding Wilson coefficients:

$$\mathcal{O}_{RR}^{(5)} = \bar{\mathcal{X}}_R^c \Omega_1 \Omega_1^T \mathcal{X}_R, \quad \frac{c_{RR}^{(5)}}{\Lambda} = -\frac{\lambda_R^2}{2M_N}, \quad (2.11)$$

$$\mathcal{O}_{LL}^{(5)} = \bar{\mathcal{X}}_L \Omega_1^* \Omega_1^\dagger \mathcal{X}_L^c, \quad \frac{c_{LL}^{(5)}}{\Lambda} = -\frac{\lambda_L^2}{2M_N}, \quad (2.12)$$

$$\mathcal{O}_{LR}^{(5)} = \bar{\mathcal{X}}_L \Omega_1^* \Omega_1^T \mathcal{X}_R, \quad \frac{c_{LR}^{(5)}}{\Lambda} = -\frac{\lambda_L \lambda_R}{M_N}, \quad (2.13)$$

and their Hermitian conjugates. The first two operators $\mathcal{O}_{RR,LL}^{(5)}$ are Weinberg type operators and violate fermion number by two units, leading to Majorana mass terms after spontaneous symmetry breaking, while $\mathcal{O}_{LR}^{(5)}$ conserves fermion number, leading to a Dirac mass term. After Ω_1 obtains a vev, $\langle \Omega_1 \rangle = (0, 0, 0, \omega_1/\sqrt{2})^T$, the 4321 group breaks down to the SM gauge group and the physical masses in eq. (2.7) are given by

$$m_\psi = m_{\mathcal{X}}, \quad (2.14)$$

$$m_{\chi_1} \simeq m_{\mathcal{X}} - \frac{(\lambda_L - \lambda_R)^2 \omega_1^2}{4M_N}, \quad (2.15)$$

$$m_{\chi_2} \simeq m_{\mathcal{X}} + \frac{(\lambda_L + \lambda_R)^2 \omega_1^2}{4M_N}. \quad (2.16)$$

Notice that for $\lambda_L \neq \lambda_R$ this UV model reproduces the desired compressed mass spectrum with the correct ordering $m_{\chi_1} < m_\psi < m_{\chi_2}$. Furthermore, the eigenstates $\chi_{1,2}$ naturally arise as a pair of pseudo-Dirac fermions since the χ_1 - χ_2 mass splitting terms $m_{L,R} = \lambda_{L,R}^2 \omega_1^2 / 2M_N$ are suppressed by the seesaw mechanism in the limit $M_N \gg \omega_1$.

Field	Type	SM QN	\mathbb{Z}_2
χ_1	Majorana	$(\mathbf{1}, \mathbf{1}, 0)$	-1
χ_2	Majorana	$(\mathbf{1}, \mathbf{1}, 0)$	-1
ψ	Dirac	$(\mathbf{3}, \mathbf{1}, 2/3)$	-1
Z'	Gauge	$(\mathbf{1}, \mathbf{1}, 0)$	+1
U_1	Gauge	$(\mathbf{3}, \mathbf{1}, 2/3)$	+1

Table 1. The new fermions and bosons we introduce in our simplified model with their quantum numbers under the SM gauge group and the stabilising \mathbb{Z}_2 symmetry.

2.3 The Simplified Model

In our analysis, we will study a simplified model motivated by the above scenario. We will parametrise the mass splittings as

$$\Delta_\psi \equiv \frac{m_\psi - m_{\chi_1}}{m_{\chi_1}}, \quad \Delta_{\chi_2} \equiv \frac{m_{\chi_2} - m_{\chi_1}}{m_{\chi_1}}, \quad (2.17)$$

focusing on the regime where $0 \leq \Delta_\psi \lesssim 0.3$, as explained in the next section, and where $\Delta_{\chi_2} \gtrsim 2\Delta_\psi$ (motivated by eqs. (2.14) to (2.16)).

The covariant derivative terms in \mathcal{L}^{DS} , eq. (2.7), contain couplings to gauge bosons which become massive after G_{NP} breaking. These will act as mediators between the dark sector and the SM. As discussed in the introduction, the B -anomalies suggest the existence of a U_1 vector leptoquark. Once this is included, closure of the algebra means that there must also be a heavy Z' [28]. Although there could be further gauge bosons, such as a coloron, we assume that these do not significantly impact the dark sector phenomenology. The complete set of new fields we introduce in our simplified model is shown in table 1. We will see that the relic abundance and LHC phenomenology is driven by χ_1 , ψ and U_1 . In the notation of ref. [58] which classifies co-annihilation models and their LHC signatures, this is model ST2 (note that [58] uses a different hyper-charge convention to the one we employ here). The interaction terms of the new gauge bosons are

$$\begin{aligned} \mathcal{L}_U^{\text{int}} &= \frac{g_U}{\sqrt{2}} U_1^{\mu,\alpha} [\beta_L^{ij} \bar{q}_L^{i,\alpha} \gamma_\mu \ell_L^j + \beta_R^{ij} \bar{d}_R^{i,\alpha} \gamma_\mu e_R^j + \beta_{D_1} \bar{\chi}_1 \gamma_\mu \psi^\alpha + \beta_{D_2} \bar{\chi}_2 \gamma_\mu \psi^\alpha] + \text{h.c.}, \quad (2.18) \\ \mathcal{L}_{Z'}^{\text{int}} &= \frac{g_{Z'}}{2\sqrt{6}} Z'^{\mu} [\zeta_q^{ij} \bar{q}_L^i \gamma_\mu q_L^j + \zeta_u^{ij} \bar{u}_R^i \gamma_\mu u_R^j + \zeta_d^{ij} \bar{d}_R^i \gamma_\mu d_R^j - 3 \zeta_\ell^{ij} \bar{\ell}_L^i \gamma_\mu \ell_L^j - 3 \zeta_e^{ij} \bar{e}_R^i \gamma_\mu e_R^j + \\ &\quad \zeta_\psi \bar{\psi} \gamma_\mu \psi + i \zeta_\chi \bar{\chi}_2 \gamma_\mu \chi_1], \quad (2.19) \end{aligned}$$

where the numerical prefactors are motivated by the 4321 model [24]. Note that the Majorana fields χ_1 and χ_2 satisfy $\bar{\chi}_i \gamma_\mu \chi_j = -\bar{\chi}_j \gamma_\mu \chi_i$ for $i, j \in \{1, 2\}$, so the vector currents $\bar{\chi}_i \gamma_\mu \chi_i$ vanish and the above Lagrangian is Hermitian.

The $\mathcal{O}(1)$ coupling g_U and the masses m_U , m_{χ_1} , m_ψ are the parameters which dominate the determination of the dark matter abundance and collider physics signatures we consider.

For these parameters, the key relation that provides a solution to the B -physics anomalies is [29]

$$g_U = (1.1 \pm 0.2) \times \left(\frac{m_U}{2 \text{TeV}} \right). \quad (2.20)$$

For the β and ζ couplings we work in the flavour basis where the $SU(2)_L$ SM fermion doublets are aligned with the down-quark sector,

$$q_L^i = \begin{pmatrix} V_{ji}^* w_L^j \\ d_L^i \end{pmatrix}, \quad \ell_L^i = \begin{pmatrix} \nu^i \\ e_L^i \end{pmatrix}, \quad (2.21)$$

where V is the CKM matrix. In this basis, motivated by the B -anomalies and minimality, we assume the following structure for the β couplings

$$\beta_L = \begin{pmatrix} 0 & 0 & \beta_L^{d\tau} \\ 0 & \beta_L^{s\mu} & \beta_L^{s\tau} \\ 0 & \beta_L^{b\mu} & 1 \end{pmatrix}, \quad \beta_R = \begin{pmatrix} 0 & 0 & 0 \\ 0 & 0 & 0 \\ 0 & 0 & -1 \end{pmatrix}, \quad \beta_{D_1} = \beta_{D_2} = 1. \quad (2.22)$$

Non-zero values for β_L^{ij} are needed to address the B -anomalies, and may arise when connecting this simplified model to UV models addressing the structure of the SM Yukawa couplings [25, 27]. While these parameters only have a marginal influence on the dark matter abundance and the collider physics signatures we consider in this work, for definiteness we take $\beta_L^{s\tau} = -\beta_L^{b\mu} \approx 0.11$ and $\beta_L^{s\mu} = -\beta_L^{d\tau} \approx 0.02$ [25].

For the Z' couplings, we take $\zeta_q^{33} = \zeta_u^{tt} = \zeta_d^{bb} = \zeta_\ell^{33} = \zeta_e^{\tau\tau} = \zeta_\psi = \zeta_\chi = 1$ and all others equal to zero. Although we will take $g_{Z'} = g_U$ and $m_{Z'} = m_U/\sqrt{2}$, these parameters do not have a significant influence on the dark matter abundance or LHC signatures considered (as long as $g_{Z'}$ isn't too large and the Z' isn't too light, as detailed below). Finally, in addition to the kinetic term for the leptoquark we also include non-minimal interactions between the leptoquark and the SM gauge fields appearing in gauge models,

$$\mathcal{L}_U \supset -\frac{1}{2} U_{1\mu\nu}^\dagger U_1^{\mu\nu} - i g_s U_{1\mu}^\dagger T^a U_{1\nu} G^{a\mu\nu} - i g_Y \frac{2}{3} U_{1\mu}^\dagger U_{1\nu} B^{\mu\nu}, \quad (2.23)$$

where $T^a = \lambda^a/2$ and λ^a ($a = 1, \dots, 8$) are the Gell-Mann matrices.

3 Dark Matter Relic Surface

We now turn to the dark matter relic abundance. The presence of the coannihilating partner, ψ , can heavily impact the relic abundance of the dark matter candidate, χ_1 . We will restrict the parameter space by insisting that the model produces the observed relic abundance via thermal freeze-out.

First, to clearly describe the physics of coannihilation, we will imagine that the masses of the dark sector (DS) particles χ_1 , χ_2 and ψ are above the electroweak scale and that the leptoquark and Z' are heavy enough not to be present during χ_1 freeze-out (we allow them to be lighter in our numerical work below). If $m_\psi, m_{\chi_2} \gg m_{\chi_1}$ then all processes connecting

χ_1 to the thermal bath are heavily suppressed. As such, χ_1 will freeze-out when relativistic and will have a relic abundance many orders of magnitude too large to match observations (it will overclose the universe). However, the situation is very different if $m_{\chi_1} \sim m_\psi \sim m_{\chi_2}$. In this case the abundances of χ_1 , χ_2 and ψ are similarly Boltzmann suppressed during freeze-out of χ_1 . The conversion processes $\text{DS SM} \rightarrow \text{DS SM}$ have one rare, heavy particle and one bath particle in the initial state, so they have a rate exponentially larger than dark sector annihilation processes $\text{DS DS} \rightarrow \text{SM SM}$, which requires two rare particles. In our model $\bar{\chi}_1\chi_1 \rightarrow \text{SM SM}$ is absent while both $\bar{\chi}_1\psi \rightarrow \text{SM SM}$ (via an s -channel leptoquark) and $\bar{\psi}\psi \rightarrow \text{SM SM}$ (via QCD processes) are efficient. This means that although χ_1 cannot efficiently annihilate with $\bar{\chi}_1$, it can annihilate with $\bar{\psi}$ or be efficiently depleted by first converting into ψ , via $\chi_1 \text{ SM} \rightarrow \psi \text{ SM}$, which then annihilates via $\bar{\psi}\psi \rightarrow \text{SM SM}$. This coannihilation effect will be relevant if the mass splitting between ψ and χ_1 is small [59],

$$\Delta_\psi \lesssim 0.3, \quad (3.1)$$

and becomes more important as Δ_ψ shrinks. Similarly, if $\Delta_{\chi_2} \lesssim 0.3$ then $\bar{\chi}_1\chi_2 \rightarrow \text{SM SM}$ via an s -channel Z' may be efficient. However, since $\Delta_{\chi_2} \gtrsim 2\Delta_\psi$, $g_{Z'} \sim g_U$ and $m_{Z'} \sim m_U$ and since the relic abundance is predominantly determined by the most efficient process (which is $\bar{\chi}_1\psi \rightarrow \text{SM SM}$ or $\bar{\psi}\psi \rightarrow \text{SM SM}$ in the parameter space of interest), χ_2 does not play an important role in setting the relic abundance. We do however keep it in our numerical work.

To accurately calculate the relic abundance of χ_1 , the Boltzmann equation must track the abundances of χ_1 , χ_2 and ψ . This coupled differential equation can be written as a single differential equation [59], which is equivalent to the usual Boltzmann equation for a single species but with the annihilation cross-section replaced by

$$\sigma_{\text{eff}} = \sum_{ij} \frac{g_i g_j}{g_{\text{eff}}^2} \sigma_{ij} (1 + \Delta_i)^{\frac{3}{2}} (1 + \Delta_j)^{\frac{3}{2}} e^{-x(\Delta_i + \Delta_j)}, \quad (3.2)$$

where $i, j \in \{\chi_1, \chi_2, \psi\}$ index the dark sector particles (note that $\Delta_{\chi_1} = 0$), g_i is the number of degrees of freedom of particle i ($g_{\chi_1} = g_{\chi_2} = 2$, $g_\psi = 4$ in our model), the cross-section is $\sigma_{ij} = \sigma(ij \rightarrow BB')$ where B and B' are particles in the thermal bath and $x = m_{\chi_1}/T$. The effective number of degrees of freedom is given by

$$g_{\text{eff}} = \sum_i g_i (1 + \Delta_i)^{\frac{3}{2}} e^{-x\Delta_i}. \quad (3.3)$$

We see that, for instance, when $\sigma_{\chi_1\psi} \gg \sigma_{\bar{\chi}_1\chi_1}$ and both Δ_ψ and g_{eff} are not too large, then

$$\sigma_{\text{eff}} \gg \sigma_{\bar{\chi}_1\chi_1}. \quad (3.4)$$

Since $\Omega_{\chi_1} h^2 \sim 1/\langle\sigma v\rangle$, coannihilation effects then reduce the relic abundance of χ_1 .

To calculate the relic abundances we use model files written with `FeynRules v2.3` [60] and solve the Boltzmann equations using `micrOMEGAs v5` [61]. In principle, Sommerfeld corrections and the effects of bound state formation lead to corrections to the perturbative

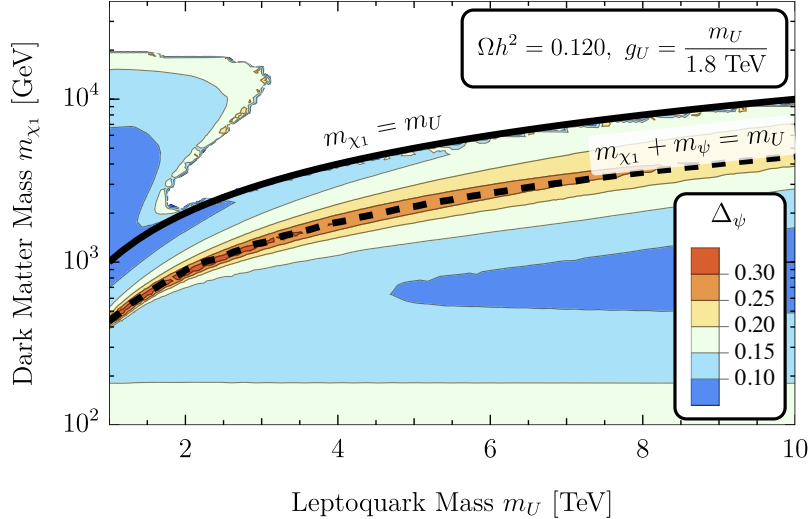


Figure 1. The mass splitting Δ_ψ that yields the observed dark matter relic abundance as a function of the leptoquark mass m_U and the dark matter mass m_{χ_1} . While we set $\Delta_{\chi_2} = 2\Delta_\psi$, $g_{Z'} = g_U$ and $m_{Z'} = m_U/\sqrt{2}$ in our numerics, the result is only weakly dependent on these parameters (as long as $\bar{\chi}_1\chi_2 \rightarrow \text{SM SM}$ via an s -channel Z' is subdominant). Below the solid black line $m_{\chi_1} < m_U$, while the dotted black line shows the resonant region where $m_{\chi_1} + m_\psi = m_U$. The observed dark matter relic abundance cannot be obtained in the white region.

cross-sections of coloured particle annihilation in the early universe. However, for the case of fermionic triplets in the TeV mass range, these corrections are negligible [62–64] and we do not include them. We use the relation between g_U and m_U given in eq. (2.20) and determine the value of the mass splitting Δ_ψ which will result in the observed relic abundance [65],

$$\Omega_{\text{DM}} h^2 = 0.120 \pm 0.001. \quad (3.5)$$

The required value of Δ_ψ is shown in fig. 1. While we set $\Delta_{\chi_2} = 2\Delta_\psi$, $g_{Z'} = g_U$ and $m_{Z'} = m_U/\sqrt{2}$, we have checked that the result is only weakly dependent on these parameters. We see that the observed relic abundance can be obtained over a large mass range of χ_1 ($100 \text{ GeV} \lesssim m_{\chi_1} \lesssim 20 \text{ TeV}$) for mass splittings in the range $0.05 \lesssim \Delta_\psi \lesssim 0.35$. We do not consider leptoquark masses below 1.5 TeV due to collider constraints, or above 10 TeV, since g_U becomes non-perturbative (due to eq. (2.20)).

We first discuss the region with $m_{\chi_1} < m_U$ (below the solid black line). Along the resonant line $m_{\chi_1} + m_\psi = m_U$ the cross-section for the s -channel process $\chi_1\psi \rightarrow \text{SM SM}$ is large and so a large mass splitting is required to achieve the observed relic abundance. For a fixed m_U , as m_{χ_1} reduces the process goes further off resonance, so a smaller mass splitting is required to compensate (to keep σ_{eff} approximately constant). This continues until $\psi\psi \rightarrow \text{SM SM}$ becomes the dominant process at small m_{χ_1} . Once this happens the required mass splitting grows as m_{χ_1} , and so m_ψ , reduces. In the region $m_U - m_\psi < m_{\chi_1} < m_U$, the mass splitting becomes smaller further from the resonance line, as the process again goes further off resonance.

When $m_{\chi_1} > m_U$ (above the solid black line), in much of the parameter space the dominant process is $\chi_1\chi_1 \rightarrow U_1U_1$ via a t -channel ψ (when $m_U \ll m_{\chi_1}$, the leptoquark is still abundant as χ_1 freezes-out, so this process can efficiently annihilate χ_1). In this case the effective cross-section, eq. (3.2), is not exponentially sensitive to Δ_ψ , so small variations in m_ψ cannot yield the observed relic abundance. This is indicated by the white region. Only when $m_U \lesssim 3 \text{ TeV}$ do the processes $\chi_1\psi \rightarrow BB'$ and $\psi\psi \rightarrow BB'$, where B and B' are bath particles, compete with $\chi_1\chi_1 \rightarrow U_1U_1$, so that Δ_ψ can be adjusted to obtain the observed relic abundance. Above $m_{\chi_1} \sim 20 \text{ TeV}$ the observed relic abundance cannot be obtained for any Δ_ψ or m_U .

4 Coloured Coannihilation Partner Phenomenology

Since the dark matter candidate in our model is a Majorana fermion, the direct and indirect detection constraints are negligible [58, 62, 66]. As such, the strongest constraints on the simplified model parameter space will come from collider searches for the new particles. Collider searches for the leptoquark and Z' have been well studied, and constrain the leptoquark to being heavier than $\sim 1.7 \text{ TeV}$ [28, 29]. Although the presence of the dark sector may weaken these limits, the leptoquark and Z' will still have significant branching ratios to SM particles. The lightest dark sector particle, the dark matter candidate χ_1 , is a gauge singlet and only couples to the SM via the heavy leptoquark and Z' , so searches for the dark matter candidate directly are challenging. However, as discussed in section 2, the coannihilation partner ψ is similar in mass to the dark matter candidate and is a colour triplet, making it directly accessible at hadron colliders. For this reason we focus on searches for ψ production.

After we fix the couplings as discussed in section 2.3, the model parameters relevant for collider searches are the masses of the dark matter candidate, m_{χ_1} , the coannihilation partner, m_ψ , and the leptoquark, m_U . In section 3 we found the ψ mass which leads to the observed dark matter relic abundance through thermal freeze-out, as shown in fig. 1. In our collider analysis we use this result to eliminate m_ψ , allowing us to present our results in the m_{χ_1} - m_U plane.

Since ψ is an unstable coloured fermion, it is important to compare its width with the QCD scale to see if it is likely to hadronize. We are primarily interested in the case where the \mathbb{Z}_2 -odd fermions are significantly heavier than the SM particles, but lighter than the U_1 leptoquark (since the LHC will not be sensitive to dark sector particles heavier than a few TeV). Due to \mathbb{Z}_2 -parity conservation, the dominant ψ decay channels are the three-body processes $\psi \rightarrow \chi_1 b \tau$ and $\psi \rightarrow \chi_1 t \nu_\tau$, which are mediated by an off-shell leptoquark. Due to the compressed spectrum, $m_\psi \sim m_{\chi_1}$, the width of ψ is expected to be small. A straightforward computation (see eq. (B.3)) yields the partial width

$$\Gamma_{\psi \rightarrow \chi_1 b \tau} \lesssim 10^{-6} \text{ GeV} \left(\frac{m_\psi}{\text{TeV}} \right)^5, \quad (4.1)$$

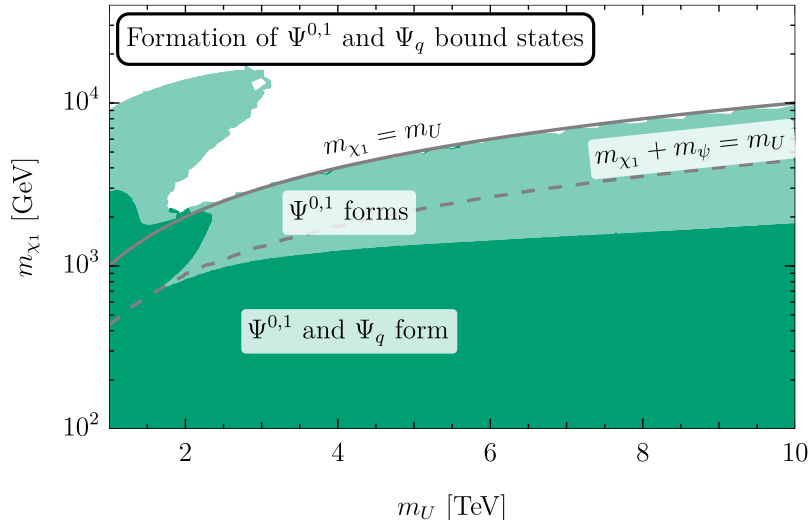


Figure 2. Regions of the $m_{\chi_1} - m_U$ plane where ψ hadronizes, with Δ_ψ fixed to yield the observed dark matter relic abundance. In the light green region the lifetime of ψ is long enough for ‘psionium’ states ($\psi\bar{\psi}$) to form, while in the dark green region formation of ‘open-psi’ mesons ($\psi\bar{q}$) also occurs.

for the coannihilation regime $\Delta_\psi < 0.3$ and for generic leptoquark couplings satisfying low energy constraints.³ These suppressed widths for a TeV scale ψ suggest that it has enough time to hadronize into QCD bound states before it decays.

4.1 Ψ -Meson Spectroscopy

There are two types of mesonic bound states: ‘psionium’ states ($\psi\bar{\psi}$) and ‘open-psi’ states ($\psi\bar{q}$), where q is a light SM quark. Their formation can be described, at leading order, by non-relativistic QCD using a modified coulomb potential similar to the hydrogen model [67], see appendix C for details. In this framework, the criteria for bound state formation is that the time it takes for the fermion pair to complete one rotation, t_R , (defined in eq. (C.4)) must be larger than their intrinsic lifetimes, in our case $\tau_\psi = \Gamma_\psi^{-1}$. In fig. 2 we show the regions of parameter space, on the relic surface, where the ψ lifetime is sufficiently long for the psionium states ($\psi\bar{\psi}$) (denoted $\Psi^{0,1}$, see below) and open-psi states ($\psi\bar{q}$) (denoted Ψ_q) to form. Note that the lifetimes of these bound states are not long enough for them to be considered stable on collider scales.

The coannihilating partner ψ thus gives rise to a rich spectrum of QCD bound states above the electroweak scale. The spectrum is expected to have a pattern similar to the bound state mesons containing charm or bottom quarks in the SM. These new heavy bound states can be classified using spin, parity, charge-conjugation and the new \mathbb{Z}_2 -parity. We use the usual notation J_\pm^{PC} with an additional \pm subscript to indicate its \mathbb{Z}_2 -parity. All psionia states are \mathbb{Z}_2 -even, and the lightest psionium states are the S -wave pseudoscalar 0_+^{-+} followed by the vector 1_+^{-} (in analogy to the η_c and J/ψ mesons in the charm sector of the SM, respectively). We name the ground state pseudoscalar state Ψ^0 and the lightest

³We obtain an expression similar to eq. (4.1) for the partial width into the $\chi_1 t \nu_\tau$ channel.

Type	Production	Decay
QCD	$gg \rightarrow \Psi^0$	$\Psi^0 \rightarrow gg$
	$gg \rightarrow \Psi^1 g$	$\Psi^1 \rightarrow ggg$
	$q\bar{q}, gg \rightarrow \Psi_q \bar{\Psi}_q$	$\Psi^1 \rightarrow \gamma gg$
EW	$q\bar{q} \rightarrow \Psi^{0,1}$	$\Psi^0 \rightarrow \gamma\gamma$
		$\Psi^1 \rightarrow q\bar{q}$
		$\Psi^1 \rightarrow \ell^+ \ell^-$
NP	$bg \rightarrow \chi_1 \Psi_q \tau^\pm$	$\Psi_q \rightarrow \chi_1 b \tau^\pm$

Table 2. The main Ψ -meson production and decay modes for each type of interaction at the LHC.

vector state Ψ^1 . The open-psi bound states ($\psi\bar{q}$), which we denote as Ψ_q , are all \mathbb{Z}_2 -odd resonances analogous to the D_q -mesons in the SM.

4.2 Collider Signatures

Given that ψ carries both colour and charge, it can be produced in large numbers at hadron colliders, mainly via QCD interactions. Single ψ production is forbidden by \mathbb{Z}_2 -parity invariance, making $pp \rightarrow \psi\bar{\psi}$ the main production mechanism at the LHC. At threshold, the pair of ψ particles will bind to form Ψ -mesons, leading to either single production of $\Psi^{0,1}$ states, or pair production of Ψ_q states. In table 2 we show the main production and decay mechanisms for $\Psi^{0,1}$ and Ψ_q at the LHC. Note that there is no QCD $q\bar{q} \rightarrow \Psi^{0,1}$ production or $\Psi^{0,1} \rightarrow q\bar{q}$ decay due to angular momentum conservation and since Ψ^1 is a colour singlet [68].

4.2.1 Search for Psionium in the Dilepton Channel

The cleanest channels for discovering the psionium states are the processes $pp \rightarrow \Psi^0 \rightarrow \gamma\gamma$ and $pp \rightarrow \Psi^1 \rightarrow \ell^+ \ell^-$, which lead to a resonant peak in the diphoton and dilepton invariant mass spectra at the mass of the psionium, $m_{\Psi^{0,1}} \approx 2m_\psi$. Since we found that the dilepton decay channel of the vector meson $pp \rightarrow \Psi^1 \rightarrow e^+ e^-, \mu^+ \mu^-$ (depicted in left panel of fig. 3) produces more stringent LHC limits, we focus on this process.⁴ The partonic cross-section is given in the narrow-width approximation by

$$\hat{\sigma}(pp \rightarrow \ell^+ \ell^-) = [\hat{\sigma}(q\bar{q} \rightarrow \Psi^1) + \hat{\sigma}(gg \rightarrow \Psi^1 g)] \times \text{BR}(\Psi^1 \rightarrow \ell^+ \ell^-). \quad (4.2)$$

In appendix D we give the respective expressions for the partonic production cross-sections and the leading order decay rates. We used the package `RunDec` [70] to take higher order loop-corrections in the running of the strong coupling into account (which is important since the process is highly sensitive to the value of the strong coupling). Finally, we convolve the partonic cross-sections with the parton distribution function (PDF) set `PDF4LHC15_nnlo_mc` [71–73]. The total cross-section is shown in fig. 4, as function of

⁴For the diphoton channel, we considered the limits imposed by the search [69].

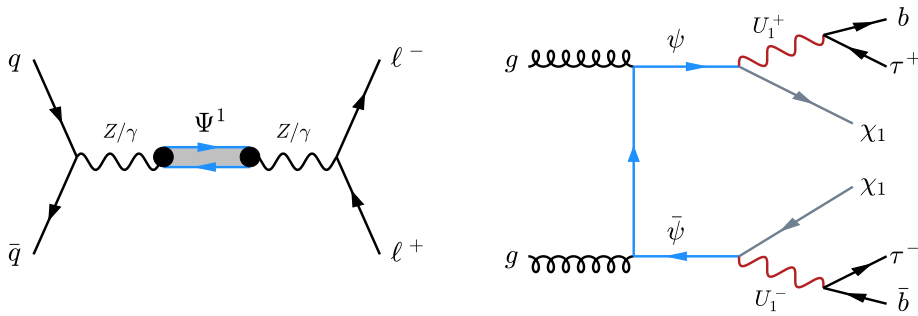


Figure 3. (Left) Electroweak production of Ψ^1 and its subsequent decay into two leptons. (Right) A representative diagram for pair production of ψ , which both decay into $b\tau\chi_1$.

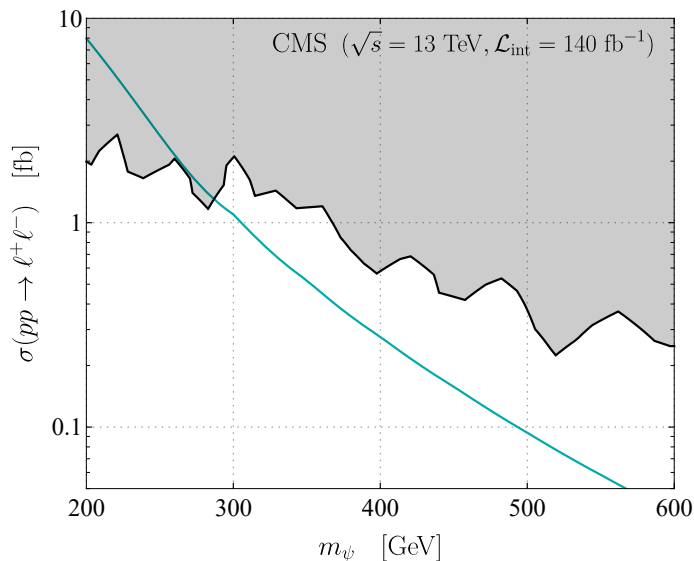


Figure 4. The total cross-section (green curve) for the signal channel $pp \rightarrow \ell^+\ell^-$, with $\ell = e, \mu$, as a function of m_ψ . The grey region is excluded by a 13 TeV CMS search with 140 fb^{-1} [74].

m_ψ . Using the experimental upper bounds on the total cross-section for vector resonances given in ref. [74], we find that this dilepton search excludes $m_\psi < 280 \text{ GeV}$. Notice that this limit is independent of the exact values of the model parameters, as long as ψ hadronizes.

4.2.2 ψ Pair Production

We now turn to pair production of Ψ_q bound states. These states predominantly decay through $\psi \rightarrow b\tau\chi_1$ or $\psi \rightarrow t\nu_\tau\chi_1$, since they are \mathbb{Z}_2 -odd, leading to collider signatures $bb\tau\tau\chi_1\chi_1$, $bt\tau\nu_\tau\chi_1\chi_1$ or $tt\nu_\tau\nu_\tau\chi_1\chi_1$. Due to the large top mass, $\psi \rightarrow \chi_1 t\nu_\tau$ is typically kinematically forbidden for dark matter masses below 1 TeV, so we focus on $\psi \rightarrow \chi_1 b\tau$ decay channel (see the right panel of fig. 3). Since $m_\psi \gg m_q$, the light quark acts as a spectator and we can assume that Ψ_q and ψ share the same mass and decay width. Therefore, in a collider environment, we may neglect the presence of the light quark altogether.

ATLAS and CMS have performed searches for pair-produced scalar leptoquarks decaying into the $b\bar{b}\tau\tau + E_T^{\text{miss}}$ final state at $\sqrt{s} = 13$ TeV with an integrated luminosity of 36.1 fb^{-1} [53–56]. Unfortunately, these searches do not set strong limits on the model since they rely on large p_T selection cuts for the reconstructed b -jets and τ -jets. The b - and τ -jet coming from ψ are expected to be relatively soft, due to the compressed spectrum $m_\psi \gtrsim m_{\chi_1}$, and therefore fail to pass the basic selection criteria for these searches. Indeed, when recasting [53–56] we found very small selection efficiencies, and these searches provided no constraints on our parameter space. In the next section we propose a dedicated search strategy for this type of compressed spectrum signatures at the LHC.

However, the failure of the visible decay products of Ψ_q to pass the typical LHC search cuts means that mono- X searches may be sensitive. The picture is that the soft (undetected) $b\tau$ pairs and hard missing transverse energy recoil against hard electroweak or QCD initial-state radiation (ISR) that does pass the selection criteria. In ref. [75], the process $pp \rightarrow Q\bar{Q} + j$ is investigated, where Q is a heavy coloured particle that decays into a dark matter candidate (and SM particles) and j is a hard (i.e., $p_T^j > 250$ GeV) ISR jet. The authors performed a recast of the ATLAS inclusive monojet search [76] and derive lower bounds on m_Q for benchmarks of different spin and colour representations. The results obtained at NLO QCD for a fermionic top-partner can be readily applied to our scenario. It is worth noticing here that the study fixes the mass gap $\Delta m = m_Q - m_{\text{DM}} \lesssim 40$ GeV in order to avoid transitions to multi-jet + MET signatures. The relevant part of the parameter space in our setup where this condition can be satisfied is $m_\psi < 400$ GeV, as can be seen in fig. 1. Coincidentally, the lower limit derived in [75] for the mass of the fermionic top-partner stands around the same value. Therefore, we conclude that inclusive monojet searches exclude ψ masses below 400 GeV at $\sqrt{s} = 13$ TeV with $\mathcal{L} = 36.1 \text{ fb}^{-1}$ of data.

4.2.3 Single ψ Production

It is possible to produce a single ψ in association with the dark matter particle χ_1 via $pp \rightarrow \chi_1\psi\tau$ (see table 2). Such production processes would directly probe the leptoquark coupling, which must be large to accommodate the B -physics anomalies. Unfortunately, these are $2 \rightarrow 3$ body transitions and are therefore heavily phase-space suppressed compared to the $2 \rightarrow 2$ processes. Moreover, the partonic initial state contains one b -quark, so this process is further suppressed by the small bottom PDF. While interesting, single ψ production modes are not expected to set competitive limits on the parameter space.

5 Dedicated Search for ψ Pairs

We propose a novel LHC search strategy for ψ pair production, specifically $pp \rightarrow \psi\bar{\psi} \rightarrow b\bar{b}\tau^-\tau^+\chi_1\chi_1$ assuming a compressed spectrum scenario, $m_\psi \gtrsim m_{\chi_1}$. We focus on the experimental signature $2j_b + \tau_h\tau_\ell + E_T^{\text{miss}}$, consisting of a pair of b -tagged jets (j_b), one τ -tagged jet coming from a hadronically decaying τ -lepton (τ_h), one light lepton e or μ coming from a leptonically decaying τ -lepton (τ_ℓ), and a large amount of missing transverse

energy (E_T^{miss}) mostly coming from the dark matter particles and τ -neutrinos.⁵ Notice that this signature is similar to the SLT (single-lepton trigger) category described in [53]. The irreducible backgrounds are dominated by $t\bar{t}$ pair production decaying into $t \rightarrow b\tau_h\nu$ and $t \rightarrow b\ell\nu$, and sub-leading contributions from Drell-Yan ($pp \rightarrow \tau_h^+\tau_\ell^- + \text{jets}$) and diboson production ($pp \rightarrow ZZ \rightarrow \tau_h^+\tau_\ell^- j_b j_b$). The main reducible backgrounds consist of processes leading to objects misidentified as τ -jets. These fake taus arise from any process generating a prompt light lepton in association with jets and b -jets, with one of the QCD jets mistagged as a hadronic τ -lepton, $j \rightarrow \tau_h$. In order to simulate the signal and background samples, we first implemented in `FeynRules` [60] the interaction Lagrangian eq. (2.18) and generated the UFO model [77] for the Monte Carlo event generator. The parton level event samples were simulated using `MadGraph5` [78] and both showering and hadronization were performed in `Pythia8` [79]. Jets were clustered using `FastJet3` [80], while object reconstruction and detector effects were simulated with `Delphes3` [81].

For the signal process, we simulated event samples for different points in the (m_{χ_1}, m_U) mass plane with the mass splitting Δ_ψ fixed by the observed relic abundance constraint, as shown in fig. 1. Moreover, the leptoquark couplings were fixed by eqs. (2.20) and (2.22) in order to satisfy the B -anomalies. For the background processes, in our analysis we only included the leading $t\bar{t}$ process given that the other irreducible backgrounds are sub-leading. Since the $j \rightarrow \tau_h$ mistagging efficiency are not easy to estimate without using data-driven techniques, we did not include these backgrounds in our analysis. Note that such backgrounds, while typically smaller than the leading $t\bar{t}$ process, are a non-negligible background that must be included in a more thorough analysis.

In the following we describe two analyses. One is a cut-based search using a single high-level observable R_T (defined below) as a signal/background discriminator, while the other is a multi-variate analysis using a BDT classifier based on multiple low-level and high-level observables.

5.1 Event Selection and Key Observables

We now describe the basic event selections used in our analyses. Jets were clustered using the anti- k_T algorithm with the standard narrow cone radius of $R = 0.4$ and candidate leptons $\ell = e, \mu$ were selected if they passed the relative isolation requirements $I_{\text{rel}} = 0.05$ within an isolation cone of radius $R_{\text{iso}} = 0.2$. In order to improve the signal acceptance, it is important to relax the transverse momentum cuts as much as possible for any of the visible reconstructed objects since these are expected to be soft, due to the compressed spectrum. In our analysis we required $p_T(j) > 20 \text{ GeV}$, $p_T(\tau_h) > 20 \text{ GeV}$, and $p_T(\ell) > 5 \text{ GeV}$ for jets, τ -jets and isolated leptons, respectively. The rapidity selections were taken to be the standard ones: $|\eta(j)| < 2.5$, $|\eta(\tau_h)| < 2.3$, and $|\eta(\ell)| < 2.5$ with isolated electrons removed from the end-cap region ($1.37 < |\eta(e)| < 1.52$). For the b -tagging and τ -tagging efficiencies we used the default values of the ATLAS card in `Delphes3`. Finally, events are selected if

⁵Signatures with two hadronic taus ($2j_b + 2\tau_h + E_T^{\text{miss}}$) can also be considered. While this channel has a larger branching ratio, it suffers from important reducible backgrounds (e.g., fake taus) that are difficult to determine using MC simulations. Estimating the LHC sensitivity of a search strategy for this signal category is therefore beyond the scope of this paper.

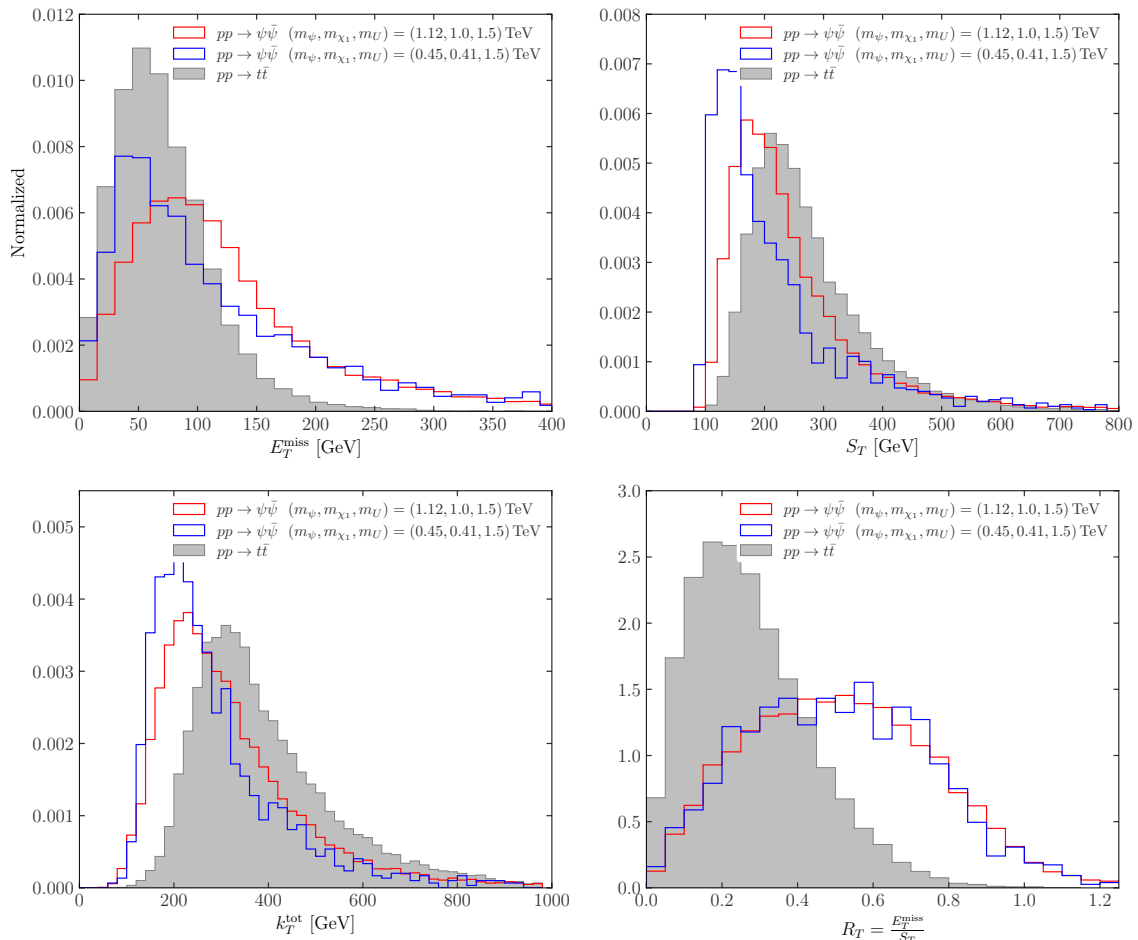


Figure 5. Normalised E_T^{miss} , S_T , k_T^{tot} and R_T event distributions for two benchmark signal processes (red, blue) and for the $t\bar{t}$ background (grey). See main text for details.

they contain two or more jets, of which at least one must be b -tagged, exactly one τ -jet and exactly one light lepton ℓ , such that the $\tau_h\ell$ pair has opposite electric charge.

After these basic selection cuts, we looked into different possible observables capable of distinguishing between the signal and the $t\bar{t}$ background. The two simplest discriminating quantities for this task are the missing transverse energy, E_T^{miss} , and the total amount of visible transverse momentum, defined as

$$S_T \equiv p_T(j_1) + p_T(j_2) + p_T(\tau_h) + p_T(\ell), \quad (5.1)$$

i.e., the scalar sum of the transverse momenta of the leading and sub-leading jets (with at least one being b -tagged), the τ -jet and the lepton. On one hand, because of the presence of the dark matter particles and neutrinos, signal events will tend to have more missing energy than $t\bar{t}$ events. On the other hand, because of the compressed spectrum, the visible energy in signal events will tend to be softer than in $t\bar{t}$ events. In the first two upper panels in fig. 5 we show these two normalised distribution for two signal benchmarks val-

ues $(m_\psi, m_{\chi_1}, m_U) = (1.12, 1.0, 1.5)$ TeV (red) and $(m_\psi, m_{\chi_1}, m_U) = (0.45, 0.41, 1.5)$ TeV (blue) that satisfy the dark matter relic abundance requirement, and the $t\bar{t}$ background (shaded grey).

In order to examine the relevance of angular information between final state objects, we also looked into the 2-point energy correlation functions. These observables are defined as

$$\mathcal{C}(x_1, \dots, x_n) = \sum_{i < j}^n p_{T_i} p_{T_j} d_{ij}^2, \quad (5.2)$$

for a set x_1, \dots, x_n of high-level reconstructed objects in the event.⁶ Here d_{ij} is the angular distance between two objects x_i and x_j , with transverse momenta p_{T_i} and p_{T_j} , respectively. We considered two possible distance functions: the azimuthal distance $\Phi_{ij} \equiv \sqrt{2(1 - \cos \Delta\phi_{ij})}$ and the plane distance $R_{ij} \equiv \sqrt{(\Delta y_{ij})^2 + (\Delta\phi_{ij})^2}$, where $\Delta y_{ij} = y_i - y_j$, $\Delta\phi_{ij} = \phi_i - \phi_j$ are determined by the rapidity y_i and azimuth angle ϕ_i of the object x_i . Notice that for $d_{ij} = \Phi_{ij}$ in eq. (5.2), each term reduces to the (squared) transverse mass M_T^2 of a pair of objects, and the observable corresponds to the square of the total transverse mass M_T^{tot} of the group of objects x_1, \dots, x_n . If instead we fix $d_{ij} = R_{ij}$, then each term in eq. (5.2) corresponds to the k_T -distance between the pairs of objects. We denote this observable k_T^{tot} and refer to it as the total k_T -distance between x_1, \dots, x_n . In fig. 5 (left lower panel) we show as an example the k_T^{tot} observable computed for the set of visible final states τ_h, ℓ^\pm, j_1 and j_2 , for signal and background. Notice that these observables containing pairwise angular correlations do not substantially improve the signal separation compared to observables such as S_T without angular information (right upper panel).⁷ M_T^{tot} , based on $d_{ij} = \Phi_{ij}$, gives very similar results.

Individually, none of the observables mentioned so far lead to a good separation between signal and background. Interestingly, much better discriminators are obtained by combining pairs of these observables. We found that the ratio between the invisible and visible total transverse momentum of the event, defined by

$$R_T \equiv \frac{E_T^{\text{miss}}}{S_T}, \quad (5.3)$$

considerably improves the signal separation compared to the individual E_T^{miss} and S_T observables. This can be seen in the lower right panel of fig. 5, where we show the normalised R_T distributions. Moreover, the shapes of the distribution for the signal process are independent of the particle masses m_ψ, m_{χ_1} , which is not the case for $E_T^{\text{miss}}, S_T, M_T^{\text{tot}}$ or k_T^{tot} . Finally, we also checked other ratios similar to eq. (5.3) by replacing the denominator with M_T^{tot} and k_T^{tot} . These ratios were found to have comparable performance to, and the same properties as, R_T . We chose to cut on R_T in our search, and we present the results in section 5.3.

⁶ n -point energy correlation functions [82] are more commonly measured between the individual constituents of a single jet.

⁷An improvement is more apparent for the $(m_\psi, m_{\chi_1}, m_U) = (1.12, 1.0, 1.5)$ benchmark (red) for which the visible final states are expected to be slightly harder and therefore more challenging to distinguish from the $t\bar{t}$ background.

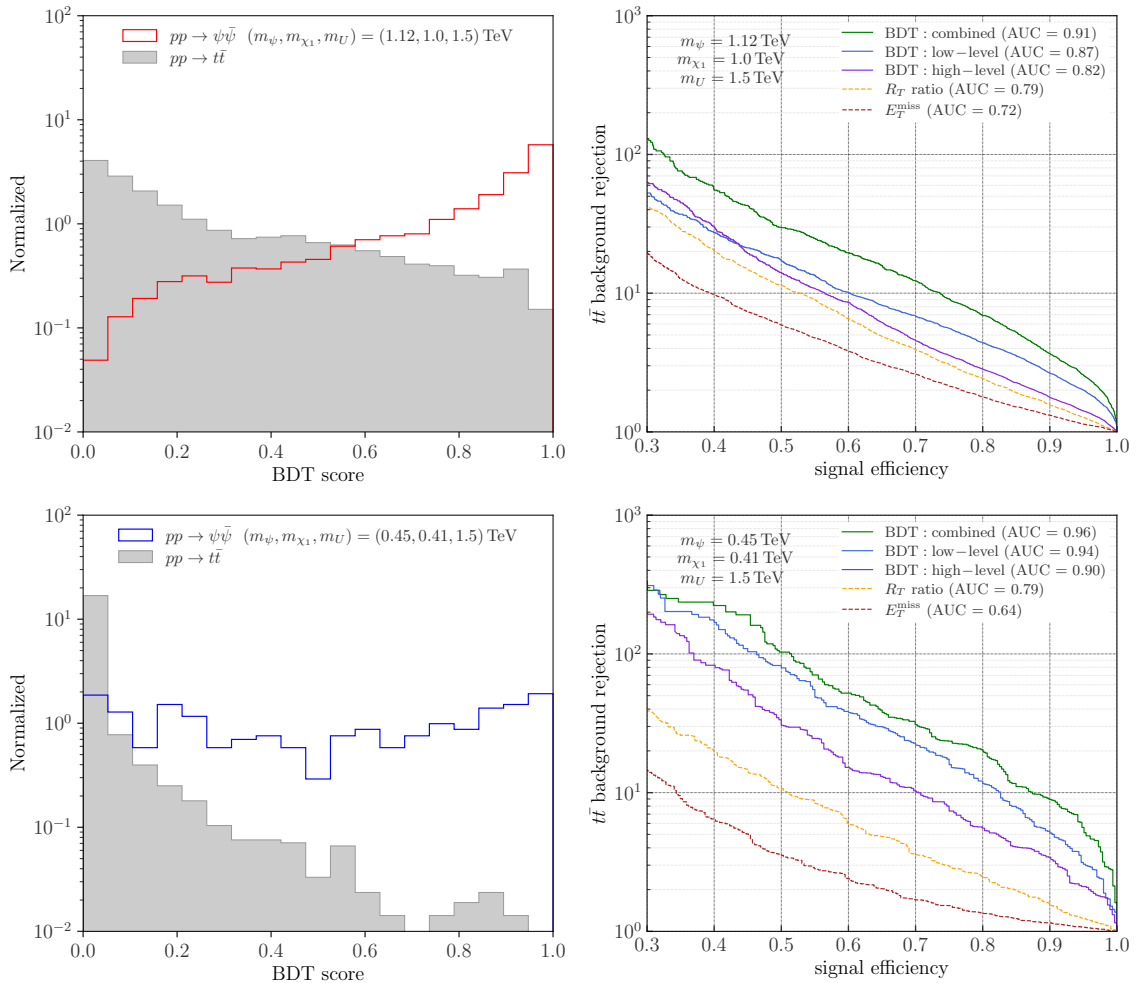


Figure 6. Left panels: BDT scores for the two different benchmark points showing signal vs background discrimination. Right panels: ROC curves for the same benchmarks showing the $t\bar{t}$ background rejection rate vs signal efficiency for three different BDT classifiers based on only high-level observables (purple curve), low-level observables (blue curve) and both high-level and low-level observables (green curve). For comparison, we also include the cut-based ROC curves for the R_T ratio (dashed yellow) and E_T^{miss} (dashed red). Better performance is achieved by ROC curves stretching towards the upper-right corner and AUC values closer to 1.

5.2 Multivariate Analysis

Given that a combination of observables (R_T) performs better than the individual ones (E_T^{miss} and S_T), we also implemented a multivariate search using a BDT classifier. After imposing the same event selections as in section 5.1, a BDT classification score was extracted using low-level and high-level observables as input variables. The low-level observables consist of the p_T and η distributions of the relevant reconstructed objects ($j_{1,2}$, τ_h and ℓ) while the high-level observables consist of E_T^{miss} , S_T , M_T^{tot} , k_T^{tot} and the R_T ratio defined in eq. (5.3).

We tested three different BDT setups: (i) the *high-level* BDT trained with only high-level observables, (ii) the *low-level* BDT trained with only low-level observables, and (iii) the *combined* BDT trained with both high-level and low-level observables. For each both signal benchmarks, we prepared an event sample with ~ 45 K labelled events and a signal to background ratio of $s/b \approx 1.2$. The samples were then split into 80% training and 20% testing sub-samples. The training was performed with XGBoost [83] using 100 trees with a maximum depth of 6, learning rate of $\eta = 0.1$ and a binary logistic for the objective function.

The resulting scores extracted from the combined BDT classifier, trained with the hyperparameters described above, is shown in the first column in fig. 5, for two signal benchmark mass points. A very clear separation between each benchmark signal and the $t\bar{t}$ background is obtained for this classifier. Furthermore, we measured the performance of the BDT classifiers using the receiving operating curves (ROC) displayed in the second column in fig. 6. There, one can observe that the three BDTs perform well (solid curves), achieving $t\bar{t}$ rejection rates above 10 for a signal efficiency of 50% and area-under-the-curve (AUC) values above ~ 0.8 . Overall, the low-level BDT (blue curve) performs better than the high-level BDT (purple curve), but the best classifier is the combined BDT (green curve) with AUCs above 0.9. The three BDTs considerably outperform the cut-based single discriminators (dashed curves). In this case the best cut-based observable was the R_T ratio which produces moderate background rejection with an AUC close to 0.8.

These results demonstrate that a BDT classifier trained on both low-level and high-level observables can improve the $t\bar{t}$ background rejection rate by at least a factor of two compared to the cut-based strategy based on the best high-level single observable, the R_T ratio.

5.3 Results

A set of signal event samples for different values of (m_{χ_1}, m_U) were generated covering the parameter space region $200 \text{ GeV} < m_{\chi_1} < 1000 \text{ GeV}$ and $1500 \text{ GeV} < m_U < 5000 \text{ GeV}$, with a rectangular grid with spacing $(\delta m_{\chi_1}, \delta m_U) = (50, 200) \text{ GeV}$. In order to get statistically significant MC samples (especially in the tails of the R_T distribution) we simulated around 1 M signal events for each mass point of the grid. For the background, we generated 500 K $t\bar{t}$ events.

For the cut-based strategy, after performing the event selections for each sample, we performed a statistical analysis using the binned R_T distribution in the interval $[0.5, 1.0]$ with a bin step of 0.1 including overflow in the last bin. Events were estimated with run-II integrated luminosity of $\mathcal{L}_{\text{int}} = 140 \text{ fb}^{-1}$ and a centre-of-mass energy of $\sqrt{s} = 13 \text{ TeV}$. In each R_T bin, we fixed a 10% uncertainty for the $t\bar{t}$ background, which is approximately the same uncertainty that was estimated for the background S_T distributions in ref. [54]. For the multivariate analysis, we trained the combined BDT on each point of the rectangular grid using the hyperparameters described above but with 50% training and 50% testing sub-samples (in order to retain enough MC events in the testing sample). We then used the binned score of the BDT classifier with 20 equidistant bins over the unit interval. Following ref. [54], we assumed a 10% background uncertainty for the BDT score. For each

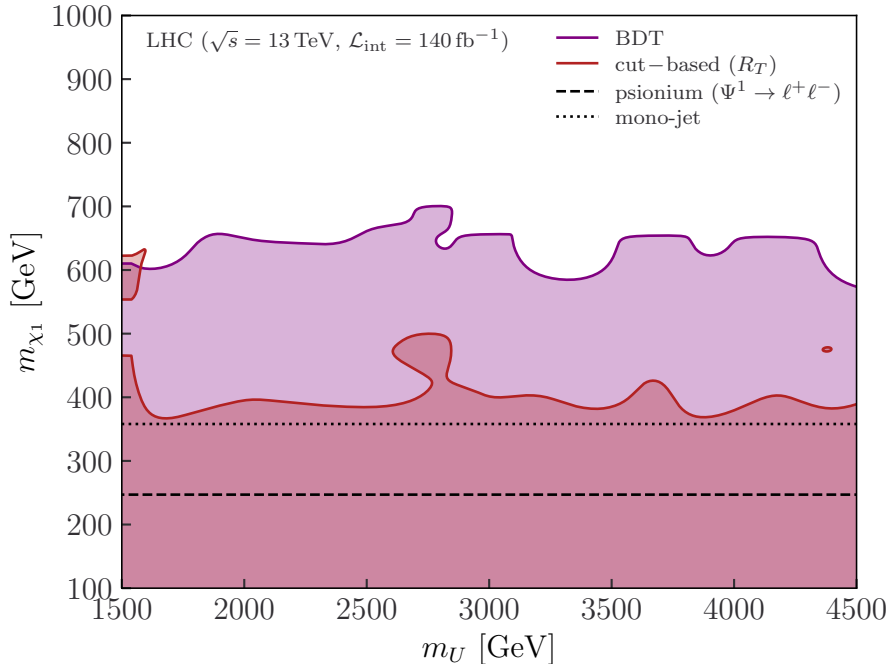


Figure 7. Exclusion limits at 95% CL for the cut-based analysis based on the R_T observable (red region) and the multivariate analysis based on a combination of low-level and high-level observables (purple region). For comparison, the psionium and monojet limits are also shown.

of the two search strategies, the expected exclusion limits were extracted at each point in the $m_{\chi_1}-m_U$ plane using the asymptotic approximation of the CL_s criteria [84, 85] with the profile likelihood ratio as test statistic. This statistical model was implemented using the `pyhf` python package [86, 87]. A mass point in the $m_{\chi_1}-m_U$ plane is excluded at 95% confidence level (CL) if $CL_s < 0.05$ is satisfied. In fig. 7 we present the final upper exclusion regions in the $m_{\chi_1}-m_U$ plane given by the red area for the cut-based analysis and the purple area for the multivariate analysis. For comparison, we have also included the model-independent limits from the psionium production $pp \rightarrow \Psi^1 \rightarrow \ell^+\ell^-$ (black dashed), as well as the expected reach of a monojet search (black dotted). We can see that both the cut-based and multivariate dedicated searches will give stronger limits than these recasted limits. Moreover, the multivariate analysis significantly outperforms the cut-based limits.

6 Conclusions

In this work we have investigated coannihilating dark matter, motivated by the vector leptoquark explanation of the B -physics anomalies. Assuming that the leptoquark is a gauge boson of a spontaneously broken gauge symmetry, and that dark matter is a fermion contained in a multiplet of that symmetry, the dark sector will also contain a coloured coannihilation partner. Furthermore, introducing UV-motivated dimension-5 operators leads to a Majorana dark matter candidate which is similar in mass to the coannihilation partner.

We determined the mass splitting between the Majorana dark matter particle χ_1 and its coannihilation partner ψ required to reproduce the observed dark matter relic abundance via thermal freeze-out (see fig. 1). Interestingly, processes with a leptoquark mediator are significantly more efficient than those with a Z' mediator. We found that the relic abundance can be satisfied for dark matter masses up to ~ 10 TeV and for leptoquark masses in the motivated range from 1.7–10 TeV. We then analysed the phenomenology of the model for the slice of parameter space which reproduces the observed relic abundance. Direct and indirect constraints are negligible as the dark matter candidate is a Majorana fermion, so collider experiments are the best probe of the parameter space.

Since leptoquark searches have been well studied and searches for the dark matter candidate in our setup are challenging, we focused on the coloured coannihilating partner, which can be pair produced with a relatively large cross-section at the LHC. The coannihilating partner lifetime is long enough for it to hadronize, forming both ‘psionium’ and ‘open-psi’ bound states. Psionium can decay via electroweak interactions into dileptons, leading to a lower bound of 280 GeV on the mass of the coannihilating partner. Open-psi predominantly decays to dark matter along with a b quark and a τ lepton via an off-shell U_1 leptoquark. Due to the compressed spectrum, the b quarks and τ leptons will be soft and may not pass selection cuts. We found that existing searches for $bb\tau\tau + E_T^{\text{miss}}$ do not place constraints on the relevant parameter space. However, monojet searches are sensitive and currently exclude coloured coannihilation partner masses below 400 GeV.

We proposed a new search strategy centred around a new observable: the ratio between visible and missing transverse energy of the process. We performed both a cut-based and a multi-variate analysis that directly probe the mass of the coloured partner, assuming LHC run-II luminosities. Using the relic surface, we determined expected limits on the dark matter mass: $m_{\chi_1} \lesssim 400$ GeV and $m_{\chi_1} \lesssim 600$ GeV for the two analyses, respectively. We therefore conclude that a multi-variate analysis would significantly improve on current limits and could probe a significant portion of viable parameter space.

Our final results are summarised in fig. 7. Although this analysis was motivated by dark matter and the B -physics anomalies, we emphasise that (i) bound state formation and decay could be relevant for other coannihilating scenarios with coloured partners, and (ii) the ratio of visible to missing transverse energy could be a powerful discriminator in scenarios with compressed spectra and long-lived invisible particles.

Finally, while our results are encouraging, a more detailed analysis performed by the LHC experimental collaborations would provide a more robust estimation of the limits. For instance, including the $2j_b + \tau_h\tau_h + E_T^{\text{miss}}$ signal category would strengthen the limits, and better accounting for mistagging rates and reducible and irreducible backgrounds would improve the accuracy of the limits. Furthermore, it would be necessary to carefully consider the trigger requirements for processes with soft final state objects, e.g., the possibility of triggering on our new observable R_T could be investigated.

7 Acknowledgements

The authors would like to thank Ben Kilminster, for asking us questions that we hope this work goes some way to answering, Gino Isidori, for collaboration in the early stages of the project and Ben Stefanek, Julie Pages, Vinicius Mikuni and Arne Reimers for useful conversations. M.J.B. was supported by the Australian Research Council and by the Swiss National Science Foundation (SNF) under contract 200021-159720. S.T. acknowledges support by MIUR grant PRIN 2017L5W2PT. D.A.F has received funding from the European Research Council (ERC) under the European Union’s Horizon 2020 research and innovation programme under grant agreement 833280 (FLAY), and by the Swiss National Science Foundation (SNF) under contract 200021-175940.

A 4321 models

We now briefly describe a SM extension that gives rise to a TeV scale $U_1 \sim (\mathbf{3}, \mathbf{1}, 2/3)$ vector leptoquark as a gauge boson with non-universal couplings to quarks and leptons. These so-called 4321 models [20–27] are defined by the gauge group

$$G_{4321} = SU(4) \times SU(3)_{c'} \times SU(2)_L \times U(1)_{Y'}, \quad (\text{A.1})$$

where $SU(2)_L$ is identified with SM weak isospin and both colour and hypercharge are diagonally embedded as $SU(3)_c \times U(1)_Y \subset SU(4) \times SU(3)_{c'} \times U(1)_{Y'}$. The breaking $G_{4321} \rightarrow G_{\text{SM}}$ is typically induced by at least two scalar fields, $\Omega_1 \sim (\bar{\mathbf{4}}, \mathbf{1}, \mathbf{1}, -1/2)$ and $\Omega_3 \sim (\bar{\mathbf{4}}, \mathbf{3}, \mathbf{1}, 1/6)$, each developing a vev around the TeV scale. A Higgs doublet $H \sim (\mathbf{1}, \mathbf{1}, \mathbf{2}, -1/2)$ is necessary for electroweak symmetry breaking. The resulting gauge sector (in addition to the SM gauge bosons) consists of a colour octet $G' \sim (\mathbf{8}, \mathbf{1}, 0)$, a colour singlet $Z' \sim (\mathbf{1}, \mathbf{1}, 0)$ and the leptoquark $U_1 \sim (\mathbf{3}, \mathbf{1}, 2/3)$, all with masses above 1 TeV.

There are two common 4321 implementations distinguished by the charge assignments of the SM matter fields:

- *(i) Standard 4321:* All three would-be SM fermion families $q_L^i, \ell_L^i, u_R^i, d_R^i, e_R^i$, are singlets under $SU(4)$ and have the usual SM charges under $SU(3)_{c'} \times SU(2)_L \times U(1)_{Y'}$. These fields therefore do not couple directly to any of the massive $SU(4)$ gauge bosons. Three vector-like fermions $\Psi_{L,R}^i \sim (\mathbf{4}, \mathbf{1}, \mathbf{2}, 0)$ are introduced in order to generate non-universal effective couplings between the SM left-handed fermions and the U_1 gauge leptoquark via fermion mixing, which arises from the Yukawa interactions $\bar{\ell}_L^i \Omega_1 \Psi_R^j$ and $\bar{q}_L^i \Omega_3 \Psi_R^j$ after spontaneous symmetry breaking. The matter content is shown in the first block for $i = 1, 2, 3$ in table 3.
- *(ii) Flavoured 4321:* In this case the would-be third family quarks and leptons are unified into $SU(4)$ multiplets $\Psi_L^3 = (q_L^3, \ell_L^3)^T$, $\Psi_R^{3+} = (t_R, \nu_R)^T$ and $\Psi_R^{3-} = (b_R, \tau_R)^T$ and couple directly to the U_1 leptoquark. The first two would-be SM generations are $SU(4)$ singlets and couplings to U_1 are induced via fermion mixing with two vector-like fermions $\Psi_{L,R}^{1,2}$, as in the standard 4321. The matter content is shown in the first and second blocks for $i = 1, 2$ in table 3.

Fields	$SU(4)$	$SU(3)_{c'}$	$SU(2)_L$	$U(1)_{Y'}$
q_L^i	1	3	2	1/6
ℓ_L^i	1	1	2	-1/2
u_R^i	1	3	1	2/3
d_R^i	1	3	1	-1/3
e_R^i	1	1	1	-1
Ψ^i	4	1	2	0
Ψ_R^{3+}	4	1	1	1/2
Ψ_L^3	4	1	2	0
Ψ_R^{3-}	4	1	1	-1/2

Table 3. Matter sector of the standard 4321 model (first block with $i = 1, 2, 3$) or the flavoured 4321 model (first and second blocks with $i = 1, 2$).

Besides the minimal field content described above, more scalar or fermion fields are sometimes necessary to satisfy additional phenomenological requirements. For instance, symmetry breaking scalars Ω_{15} transforming in the adjoint representation **15** of $SU(4)$ can be included in order to induce mass splittings between gauge bosons and fermion components [24, 25]. These fields will couple to $SU(4)$ fundamentals as $\bar{\Psi}\Omega_{15}\Psi$ and a vev along the $T^{15} = \text{diag}(1, 1, 1, -3)/\sqrt{6}$ generator will lead to a mass splitting of order $\langle\Omega_{15}\rangle$ between the coloured and colourless components of Ψ . Other 4321 matter extensions require the presence of fermion singlets (**1, 1, 1, 0**) that give rise to light Majorana neutrinos through the inverse seesaw mechanism [22, 88]. Finally, the 4321 models can be viewed as the low-energy limit of a more fundamental theory, such as the Pati-Salam cube model (PS³) [23] (which can be embedded into a warped 5D construction [88, 89]), the twin Pati-Salam model [27] or strongly coupled models with extended hypercolour [26].

B Partial Width Formulae

The tree-level partial decay width of the U_1 vector leptoquark into massive SM quarks and leptons is

$$\Gamma_{U_1 \rightarrow q_i \ell_j} = g_U^2 \left(|\beta_L^{ij}|^2 + |\beta_R^{ij}|^2 \right) \frac{\lambda(m_U^2, m_q^2, m_\ell^2)}{48\pi m_U} \left[1 - \frac{m_q^2 + m_\ell^2}{2m_U^2} - \frac{(m_q^2 - m_\ell^2)^2}{2m_U^4} \right], \quad (\text{B.1})$$

while the partial width into final state dark vector-like fermions is

$$\Gamma_{U \rightarrow \psi \chi} = g_U^2 |\beta_D|^2 \frac{\lambda(m_U^2, m_\psi^2, m_{\chi_1}^2)}{24\pi m_U} \left[1 - \frac{m_\psi^2 + m_{\chi_1}^2 - 6m_\psi m_{\chi_1}}{2m_U^2} - \frac{(m_\psi^2 - m_{\chi_1}^2)^2}{2m_U^4} \right], \quad (\text{B.2})$$

where we have used Källén's function $\lambda(x, y, z) \equiv \sqrt{x^2 + y^2 + z^2 - 2xy - 2yz - 2zx}$.

In the limit where the \mathbb{Z}_2 -odd particles are significantly heavier than the SM particles and lighter than the leptoquark, the ψ width into $\chi_1 b \tau$ is

$$\Gamma_{\psi \rightarrow \chi_1 b \tau} = \frac{g_U^4 |\beta_d|^2 (|\beta_L|^2 + |\beta_R|^2) m_\psi^5}{3072 \pi^3 M_U^4} f(m_{\chi_1}/m_\psi) + \mathcal{O}(M_U^{-6}), \quad (\text{B.3})$$

where $f(x) \equiv 1 - 2x - 8x^2 - 18x^3 + 18x^5 + 8x^6 + 2x^7 - x^8 - 24x^3(x^2 + x + 1) \log x \rightarrow 0$ as $x \rightarrow 1$. In case of a compressed spectrum $m_{\chi_1} \sim m_\psi$, $f(m_{\chi_1}/m_\psi) \ll 1$ and the width is significantly suppressed.

C Bound State Formation

To describe the bound states we use non-relativistic QCD with a modified-hydrogenic model of a single-gluon exchange potential [67]. For coloured particles of mass $m \gg \Lambda_{\text{QCD}}$, the potential takes the Coulombic form,

$$V(r) = -C \frac{\bar{\alpha}_s}{r}, \quad (\text{C.1})$$

where C is a colour factor. For a colourless bound state C is simply the quadratic Casimir of the constituent particles (i.e., $C = 4/3$ for the psionium). We define

$$\bar{\alpha}_s = \alpha_s(r_B^{-1}), \quad (\text{C.2})$$

as the running strong coupling evaluated at the scale of the average distance r_B between the two constituents. This distance is of the order of the Bohr radius $a_0 = 1/(C\bar{\alpha}_s\mu)$, where μ is the reduced mass of the system. More precisely, for an S -wave ground state $r_B = \sqrt{3}a_0$.

Bound states form if the revolution time, t_R , is larger than the lifetime of the coloured particles. Combining the ground state energy

$$E_1 = -\frac{C^2 \bar{\alpha}_s^2 \mu}{2}. \quad (\text{C.3})$$

with the virial theorem yields

$$t_R = \frac{2\pi}{C^2 \bar{\alpha}_s^2 \mu}. \quad (\text{C.4})$$

D Production and Decay Rate of Psionium Ψ^1

To determine the production cross-sections and decay widths of Ψ^1 we follow a generalisation of the results that apply to quarks and quarkonia [68]. The partial width for Ψ^1 decaying into a final state X can be written as

$$\Gamma(\Psi^1 \rightarrow X) \rightarrow \Gamma(\psi\bar{\psi} \rightarrow X) |\Psi(0)|^2, \quad (\text{D.1})$$

where $\Psi(0)$ is the wavefunction at origin for the ground state of the bound system and $\Gamma(\psi\bar{\psi} \rightarrow X)$ is the corresponding process with a free pair of ψ and $\bar{\psi}$ in the initial state. In the modified-hydrogenic model, we obtain the following wavefunction

$$|\Psi(0)|^2 = \frac{1}{\pi} \left(\frac{CM\bar{\alpha}_s}{4} \right)^3, \quad (\text{D.2})$$

where M is the psionium mass.

The leading production mechanisms of Ψ^1 are:

- i) **Electroweak production from $q\bar{q}$.** In the approximation that the psionium mass M is much larger than the Z boson mass, we may write the electroweak cross-section via an s -channel photon or Z boson as

$$\sigma(q\bar{q} \rightarrow \Psi) = \frac{\pi^2}{108} D_R C_R^3 Q^2 \frac{\alpha^2 \bar{\alpha}_s^3}{\cos^4 \theta_W} \left(17 \sum_{q=u,c} + 5 \sum_{q=d,s,b} \right) \frac{\mathcal{L}_{q\bar{q}}(M^2)}{M^2}, \quad (\text{D.3})$$

where $D_R = 3$, $C_R = 4/3$ and $Q = 2/3$. The parton luminosity for a pair of partons a and b is defined as

$$\mathcal{L}_{ab}(\hat{s}) = \frac{\hat{s}}{s} \int_{\hat{s}/s}^1 \frac{dx}{x} f_{a/p}(x) f_{b/p}\left(\frac{\hat{s}}{xs}\right), \quad (\text{D.4})$$

where $f_{a,b/p}$ are the relevant PDFs and \sqrt{s} is the collider centre-of-mass energy.

- ii) **Production in association with a gluon.** The cross-section for production in association with a gluon is

$$\sigma(gg \rightarrow \Psi^1 g) = \frac{5\pi}{192 m^2} \frac{C_R^3}{D_R} \alpha_s^3 \bar{\alpha}_s^3 \int_0^1 dx_1 \int_0^1 dx_2 f_{g/p}(x_1) f_{g/p}(x_2) I\left(\frac{x_1 x_2 s}{M^2}\right), \quad (\text{D.5})$$

where

$$I(x) = \theta(x-1) \left[\frac{2}{x^2} \left(\frac{x+1}{x-1} - \frac{2x \ln x}{(x-1)^2} \right) + \frac{2(x-1)}{x(x+1)^2} + \frac{4 \ln x}{(x+1)^3} \right]. \quad (\text{D.6})$$

Production in association with a photon or a Z boson is subleading and not considered here.

For $m_\psi \approx 500$ GeV and $\sqrt{s} = 13$ TeV, the electroweak production constitutes almost 80% of the total cross-section, due to the running of the couplings and the phase-space suppression of $gg \rightarrow \Psi^1 g$.

To determine the cross-section eq. (4.2), we need to compute the branching fraction of the Ψ^1 bound state into the following states:

- i) **SM fermions.** The decay can proceed through a photon or a Z boson and the rate for fermions f_L, f_R is given by

$$\Gamma_{\Psi^1 \rightarrow f\bar{f}} = \frac{n_c}{12} D_R C_R^3 \sum_{\sigma=R,L} \left(\frac{Y_{f\sigma} Y}{\cos^2 \theta_W} \right)^2 \alpha^2 \bar{\alpha}_s^3 m, \quad (\text{D.7})$$

where $n_c = 1$ for leptons and 3 for quarks.

- ii) *ggg* or γgg . The decay rates to three gauge bosons (which leads to the bulk of the hadronic decay modes) are

$$\Gamma_{\Psi^1 \rightarrow ggg} = \frac{5(\pi^2 - 9)}{27\pi} \frac{C_R^3}{D_R} \alpha_s^3 \bar{\alpha}_s^3 m, \quad (\text{D.8})$$

$$\Gamma_{\Psi^1 \rightarrow \gamma gg} = \frac{(\pi^2 - 9)}{12\pi} C_R^5 D_R Q^2 \alpha \alpha_s^2 \bar{\alpha}_s^3 m. \quad (\text{D.9})$$

Assuming that there are no other decays with considerable rates, the branching ratio to any single flavor of leptons is around 10%.

References

- [1] G. Bertone, D. Hooper, and J. Silk, *Particle dark matter: Evidence, candidates and constraints*, *Phys. Rept.* **405** (2005) 279–390, [[hep-ph/0404175](#)].
- [2] G. Hiller and M. Schmaltz, *R_K and future $b \rightarrow s\ell\ell$ physics beyond the standard model opportunities*, *Phys. Rev. D* **90** (2014) 054014, [[arXiv:1408.1627](#)].
- [3] B. Gripaios, M. Nardecchia, and S. A. Renner, *Composite leptoquarks and anomalies in B -meson decays*, *JHEP* **05** (2015) 006, [[arXiv:1412.1791](#)].
- [4] R. Alonso, B. Grinstein, and J. Martin Camalich, *Lepton universality violation and lepton flavor conservation in B -meson decays*, *JHEP* **10** (2015) 184, [[arXiv:1505.05164](#)].
- [5] S. Fajfer and N. Košnik, *Vector leptoquark resolution of R_K and $R_{D^{(*)}}$ puzzles*, *Phys. Lett. B* **755** (2016) 270–274, [[arXiv:1511.06024](#)].
- [6] L. Calibbi, A. Crivellin, and T. Ota, *Effective Field Theory Approach to $b \rightarrow s\ell\ell^{(\prime)}$, $B \rightarrow K^{(*)}\nu\bar{\nu}$ and $B \rightarrow D^{(*)}\tau\nu$ with Third Generation Couplings*, *Phys. Rev. Lett.* **115** (2015) 181801, [[arXiv:1506.02661](#)].
- [7] M. Bauer and M. Neubert, *Minimal Leptoquark Explanation for the $R_{D^{(*)}}$, R_K , and $(g-2)_\mu$ Anomalies*, *Phys. Rev. Lett.* **116** (2016), no. 14 141802, [[arXiv:1511.01900](#)].
- [8] R. Barbieri, G. Isidori, A. Pattori, and F. Senia, *Anomalies in B -decays and $U(2)$ flavour symmetry*, *Eur. Phys. J. C* **76** (2016), no. 2 67, [[arXiv:1512.01560](#)].
- [9] D. A. Faroughy, A. Greljo, and J. F. Kamenik, *Confronting lepton flavor universality violation in B decays with high- p_T tau lepton searches at LHC*, *Phys. Lett. B* **764** (2017) 126–134, [[arXiv:1609.07138](#)].
- [10] D. Bečirević, S. Fajfer, N. Košnik, and O. Sumensari, *Leptoquark model to explain the B -physics anomalies, R_K and R_D* , *Phys. Rev. D* **94** (2016), no. 11 115021, [[arXiv:1608.08501](#)].
- [11] B. Bhattacharya, A. Datta, J.-P. Guévin, D. London, and R. Watanabe, *Simultaneous Explanation of the R_K and $R_{D^{(*)}}$ Puzzles: a Model Analysis*, *JHEP* **01** (2017) 015, [[arXiv:1609.09078](#)].
- [12] N. Assad, B. Fornal, and B. Grinstein, *Baryon Number and Lepton Universality Violation in Leptoquark and Diqark Models*, *Phys. Lett. B* **777** (2018) 324–331, [[arXiv:1708.06350](#)].

- [13] L. Calibbi, A. Crivellin, and T. Li, *Model of vector leptoquarks in view of the B-physics anomalies*, *Phys. Rev. D* **98** (2018), no. 11 115002, [[arXiv:1709.00692](#)].
- [14] M. Blanke and A. Crivellin, *B Meson Anomalies in a Pati-Salam Model within the Randall-Sundrum Background*, *Phys. Rev. Lett.* **121** (2018), no. 1 011801, [[arXiv:1801.07256](#)].
- [15] D. Bečirević, I. Doršner, S. Fajfer, N. Košnik, D. A. Faroughy, and O. Sumensari, *Scalar leptoquarks from grand unified theories to accommodate the B-physics anomalies*, *Phys. Rev. D* **98** (2018), no. 5 055003, [[arXiv:1806.05689](#)].
- [16] J. Kumar, D. London, and R. Watanabe, *Combined Explanations of the $b \rightarrow s\mu^+\mu^-$ and $b \rightarrow c\tau^-\bar{\nu}$ Anomalies: a General Model Analysis*, *Phys. Rev. D* **99** (2019), no. 1 015007, [[arXiv:1806.07403](#)].
- [17] D. Buttazzo, A. Greljo, G. Isidori, and D. Marzocca, *B-physics anomalies: a guide to combined explanations*, *JHEP* **11** (2017) 044, [[arXiv:1706.07808](#)].
- [18] A. Angelescu, D. Bečirević, D. A. Faroughy, and O. Sumensari, *Closing the window on single leptoquark solutions to the B-physics anomalies*, *JHEP* **10** (2018) 183, [[arXiv:1808.08179](#)].
- [19] A. Angelescu, D. Bečirević, D. A. Faroughy, F. Jaffredo, and O. Sumensari, *Single leptoquark solutions to the B-physics anomalies*, *Phys. Rev. D* **104** (2021), no. 5 055017, [[arXiv:2103.12504](#)].
- [20] L. Di Luzio, A. Greljo, and M. Nardecchia, *Gauge leptoquark as the origin of B-physics anomalies*, *Phys. Rev. D* **96** (2017), no. 11 115011, [[arXiv:1708.08450](#)].
- [21] M. Bordone, C. Cornella, J. Fuentes-Martin, and G. Isidori, *A three-site gauge model for flavor hierarchies and flavor anomalies*, *Phys. Lett. B* **779** (2018) 317–323, [[arXiv:1712.01368](#)].
- [22] A. Greljo and B. A. Stefanek, *Third family quark–lepton unification at the TeV scale*, *Phys. Lett. B* **782** (2018) 131–138, [[arXiv:1802.04274](#)].
- [23] M. Bordone, C. Cornella, J. Fuentes-Martin, and G. Isidori, *Low-energy signatures of the PS^3 model: from B-physics anomalies to LFV*, *JHEP* **10** (2018) 148, [[arXiv:1805.09328](#)].
- [24] L. Di Luzio, J. Fuentes-Martin, A. Greljo, M. Nardecchia, and S. Renner, *Maximal Flavour Violation: a Cabibbo mechanism for leptoquarks*, *JHEP* **11** (2018) 081, [[arXiv:1808.00942](#)].
- [25] C. Cornella, J. Fuentes-Martin, and G. Isidori, *Revisiting the vector leptoquark explanation of the B-physics anomalies*, *JHEP* **07** (2019) 168, [[arXiv:1903.11517](#)].
- [26] J. Fuentes-Martin and P. Stangl, *Third-family quark-lepton unification with a fundamental composite Higgs*, *Phys. Lett. B* **811** (2020) 135953, [[arXiv:2004.11376](#)].
- [27] S. F. King, *Twin Pati-Salam theory of flavour with a TeV scale vector leptoquark*, [[arXiv:2106.03876](#)].
- [28] M. J. Baker, J. Fuentes-Martin, G. Isidori, and M. König, *High- p_T signatures in vector-leptoquark models*, *Eur. Phys. J. C* **79** (2019), no. 4 334, [[arXiv:1901.10480](#)].
- [29] C. Cornella, D. A. Faroughy, J. Fuentes-Martin, G. Isidori, and M. Neubert, *Reading the footprints of the B-meson flavor anomalies*, [[arXiv:2103.16558](#)].
- [30] D. Aristizabal Sierra, F. Staub, and A. Vicente, *Shedding light on the $b \rightarrow s$ anomalies with a dark sector*, *Phys. Rev. D* **92** (2015), no. 1 015001, [[arXiv:1503.06077](#)].

- [31] G. Bélanger, C. Delaunay, and S. Westhoff, *A Dark Matter Relic From Muon Anomalies*, *Phys. Rev. D* **92** (2015) 055021, [[arXiv:1507.06660](#)].
- [32] J. Kawamura, S. Okawa, and Y. Omura, *Interplay between the $b \rightarrow s\ell\ell$ anomalies and dark matter physics*, *Phys. Rev. D* **96** (2017), no. 7 075041, [[arXiv:1706.04344](#)].
- [33] P. Ko, T. Nomura, and H. Okada, *A flavor dependent gauge symmetry, Predictive radiative seesaw and LHCb anomalies*, *Phys. Lett. B* **772** (2017) 547–552, [[arXiv:1701.05788](#)].
- [34] K. Fuyuto, H.-L. Li, and J.-H. Yu, *Implications of hidden gauged $U(1)$ model for B anomalies*, *Phys. Rev. D* **97** (2018), no. 11 115003, [[arXiv:1712.06736](#)].
- [35] J. M. Cline and J. M. Cornell, *$R(K^{(*)})$ from dark matter exchange*, *Phys. Lett. B* **782** (2018) 232–237, [[arXiv:1711.10770](#)].
- [36] A. Azatov, D. Barducci, D. Ghosh, D. Marzocca, and L. Ubaldi, *Combined explanations of B -physics anomalies: the sterile neutrino solution*, *JHEP* **10** (2018) 092, [[arXiv:1807.10745](#)].
- [37] S.-M. Choi, Y.-J. Kang, H. M. Lee, and T.-G. Ro, *Lepto-Quark Portal Dark Matter*, *JHEP* **10** (2018) 104, [[arXiv:1807.06547](#)].
- [38] S. Singirala, S. Sahoo, and R. Mohanta, *Exploring dark matter, neutrino mass and $R_{K^{(*)},\phi}$ anomalies in $L_\mu - L_\tau$ model*, *Phys. Rev. D* **99** (2019), no. 3 035042, [[arXiv:1809.03213](#)].
- [39] C. Hati, G. Kumar, J. Orloff, and A. M. Teixeira, *Reconciling B -meson decay anomalies with neutrino masses, dark matter and constraints from flavour violation*, *JHEP* **11** (2018) 011, [[arXiv:1806.10146](#)].
- [40] A. Falkowski, S. F. King, E. Perdomo, and M. Pierre, *Flavourful Z' portal for vector-like neutrino Dark Matter and $R_{K^{(*)}}$* , *JHEP* **08** (2018) 061, [[arXiv:1803.04430](#)].
- [41] S. Baek and C. Yu, *Dark matter for $b \rightarrow s\mu^+\mu^-$ anomaly in a gauged $U(1)_X$ model*, *JHEP* **11** (2018) 054, [[arXiv:1806.05967](#)].
- [42] P. T. P. Hutaauruk, T. Nomura, H. Okada, and Y. Orikasa, *Dark matter and B -meson anomalies in a flavor dependent gauge symmetry*, *Phys. Rev. D* **99** (2019), no. 5 055041, [[arXiv:1901.03932](#)].
- [43] S. Trifinopoulos, *B -physics anomalies: The bridge between R -parity violating supersymmetry and flavored dark matter*, *Phys. Rev. D* **100** (2019), no. 11 115022, [[arXiv:1904.12940](#)].
- [44] D. Guadagnoli, M. Reboud, and P. Stangl, *The Dark Side of $4\beta\beta$* , *JHEP* **10** (2020) 084, [[arXiv:2005.10117](#)].
- [45] A. Carvunis, D. Guadagnoli, M. Reboud, and P. Stangl, *Composite Dark Matter and a horizontal symmetry*, *JHEP* **02** (2021) 056, [[arXiv:2007.11931](#)].
- [46] D. Huang, A. P. Morais, and R. Santos, *Anomalies in B -meson decays and the muon $g - 2$ from dark loops*, *Phys. Rev. D* **102** (2020), no. 7 075009, [[arXiv:2007.05082](#)].
- [47] F. D’Eramo, N. Košnik, F. Pobbe, A. Smolkovič, and O. Sumensari, *Leptoquarks and real singlets: A richer scalar sector behind the origin of dark matter*, *Phys. Rev. D* **104** (2021), no. 1 015035, [[arXiv:2012.05743](#)].
- [48] G. Arcadi, L. Calibbi, M. Fedele, and F. Mescia, *Systematic approach to B -physics anomalies and t -channel dark matter*, [[arXiv:2103.09835](#)].
- [49] M. Becker, D. Döring, S. Karmakar, and H. Päs, *Fermionic Singlet Dark Matter in One-Loop Solutions to the R_K Anomaly: A Systematic Study*, [[arXiv:2103.12043](#)].

- [50] G. Arcadi, L. Calibbi, M. Fedele, and F. Mescia, *Muon $g - 2$ and B -anomalies from Dark Matter*, *Phys. Rev. Lett.* **127** (2021), no. 6 061802, [[arXiv:2104.03228](#)].
- [51] J. C. Pati and A. Salam, *Lepton Number as the Fourth Color*, *Phys. Rev. D* **10** (1974) 275–289. [Erratum: *Phys.Rev.D* 11, 703–703 (1975)].
- [52] A. De Simone, V. Sanz, and H. P. Sato, *Pseudo-Dirac Dark Matter Leaves a Trace*, *Phys. Rev. Lett.* **105** (2010) 121802, [[arXiv:1004.1567](#)].
- [53] **ATLAS** Collaboration, M. Aaboud et al., *Search for resonant and non-resonant Higgs boson pair production in the $b\bar{b}\tau^+\tau^-$ decay channel in pp collisions at $\sqrt{s} = 13$ TeV with the ATLAS detector*, *Phys. Rev. Lett.* **121** (2018), no. 19 191801, [[arXiv:1808.00336](#)]. [Erratum: *Phys.Rev.Lett.* 122, 089901 (2019)].
- [54] **ATLAS** Collaboration, M. Aaboud et al., *Searches for third-generation scalar leptoquarks in $\sqrt{s} = 13$ TeV pp collisions with the ATLAS detector*, *JHEP* **06** (2019) 144, [[arXiv:1902.08103](#)].
- [55] **CMS** Collaboration, A. M. Sirunyan et al., *Search for a singly produced third-generation scalar leptoquark decaying to a τ lepton and a bottom quark in proton-proton collisions at $\sqrt{s} = 13$ TeV*, *JHEP* **07** (2018) 115, [[arXiv:1806.03472](#)].
- [56] **CMS** Collaboration, A. M. Sirunyan et al., *Search for heavy neutrinos and third-generation leptoquarks in hadronic states of two τ leptons and two jets in proton-proton collisions at $\sqrt{s} = 13$ TeV*, *JHEP* **03** (2019) 170, [[arXiv:1811.00806](#)].
- [57] D. Tucker-Smith and N. Weiner, *Inelastic dark matter*, *Phys. Rev. D* **64** (2001) 043502, [[hep-ph/0101138](#)].
- [58] M. J. Baker et al., *The Coannihilation Codex*, *JHEP* **12** (2015) 120, [[arXiv:1510.03434](#)].
- [59] K. Griest and D. Seckel, *Three exceptions in the calculation of relic abundances*, *Phys. Rev. D* **43** (1991) 3191–3203.
- [60] A. Alloul, N. D. Christensen, C. Degrande, C. Duhr, and B. Fuks, *FeynRules 2.0 - A complete toolbox for tree-level phenomenology*, *Comput. Phys. Commun.* **185** (2014) 2250–2300, [[arXiv:1310.1921](#)].
- [61] G. Bélanger, F. Boudjema, A. Goudelis, A. Pukhov, and B. Zaldivar, *micrOMEGAs5.0 : Freeze-in*, *Comput. Phys. Commun.* **231** (2018) 173–186, [[arXiv:1801.03509](#)].
- [62] M. Buschmann, S. El Hedri, A. Kaminska, J. Liu, M. de Vries, X.-P. Wang, F. Yu, and J. Zurita, *Hunting for dark matter coannihilation by mixing dijet resonances and missing transverse energy*, *JHEP* **09** (2016) 033, [[arXiv:1605.08056](#)].
- [63] W.-Y. Keung, I. Low, and Y. Zhang, *Reappraisal of dark matter co-annihilating with a top or bottom partner*, *Phys. Rev. D* **96** (2017), no. 1 015008, [[arXiv:1703.02977](#)].
- [64] S. El Hedri, A. Kaminska, M. de Vries, and J. Zurita, *Simplified Phenomenology for Colored Dark Sectors*, *JHEP* **04** (2017) 118, [[arXiv:1703.00452](#)].
- [65] **Planck** Collaboration, N. Aghanim et al., *Planck 2018 results. VI. Cosmological parameters*, *Astron. Astrophys.* **641** (2020) A6, [[arXiv:1807.06209](#)]. [Erratum: *Astron.Astrophys.* 652, C4 (2021)].
- [66] M. J. Baker and A. Thamm, *Leptonic WIMP Coannihilation and the Current Dark Matter Search Strategy*, *JHEP* **10** (2018) 187, [[arXiv:1806.07896](#)].
- [67] N. Fabiano, *Top mesons*, *Eur. Phys. J. C* **2** (1998) 345–350, [[hep-ph/9704261](#)].

- [68] Y. Kats and M. J. Strassler, *Probing Colored Particles with Photons, Leptons, and Jets*, *JHEP* **11** (2012) 097, [[arXiv:1204.1119](#)]. [Erratum: *JHEP* 07, 009 (2016)].
- [69] CMS Collaboration, A. M. Sirunyan et al., *Search for physics beyond the standard model in high-mass diphoton events from proton-proton collisions at $\sqrt{s} = 13$ TeV*, *Phys. Rev. D* **98** (2018), no. 9 092001, [[arXiv:1809.00327](#)].
- [70] K. G. Chetyrkin, J. H. Kuhn, and M. Steinhauser, *RunDec: A Mathematica package for running and decoupling of the strong coupling and quark masses*, *Comput. Phys. Commun.* **133** (2000) 43–65, [[hep-ph/0004189](#)].
- [71] L. A. Harland-Lang, A. D. Martin, P. Motylinski, and R. S. Thorne, *Parton distributions in the LHC era: MMHT 2014 PDFs*, *Eur. Phys. J. C* **75** (2015), no. 5 204, [[arXiv:1412.3989](#)].
- [72] NNPDF Collaboration, R. D. Ball et al., *Parton distributions for the LHC Run II*, *JHEP* **04** (2015) 040, [[arXiv:1410.8849](#)].
- [73] J. Butterworth et al., *PDF4LHC recommendations for LHC Run II*, *J. Phys. G* **43** (2016) 023001, [[arXiv:1510.03865](#)].
- [74] CMS Collaboration, *Search for a narrow resonance in high-mass dilepton final states in proton-proton collisions using 140 fb^{-1} of data at $\sqrt{s} = 13$ TeV*, .
- [75] A. Chakraborty, S. Kuttimalai, S. H. Lim, M. M. Nojiri, and R. Ruiz, *Monojet Signatures from Heavy Colored Particles: Future Collider Sensitivities and Theoretical Uncertainties*, *Eur. Phys. J. C* **78** (2018), no. 8 679, [[arXiv:1805.05346](#)].
- [76] ATLAS Collaboration, M. Aaboud et al., *Search for dark matter and other new phenomena in events with an energetic jet and large missing transverse momentum using the ATLAS detector*, *JHEP* **01** (2018) 126, [[arXiv:1711.03301](#)].
- [77] C. Degrande, C. Duhr, B. Fuks, D. Grellscheid, O. Mattelaer, and T. Reiter, *UFO - The Universal FeynRules Output*, *Comput. Phys. Commun.* **183** (2012) 1201–1214, [[arXiv:1108.2040](#)].
- [78] J. Alwall, R. Frederix, S. Frixione, V. Hirschi, F. Maltoni, O. Mattelaer, H. S. Shao, T. Stelzer, P. Torrielli, and M. Zaro, *The automated computation of tree-level and next-to-leading order differential cross sections, and their matching to parton shower simulations*, *JHEP* **07** (2014) 079, [[arXiv:1405.0301](#)].
- [79] T. Sjöstrand, S. Ask, J. R. Christiansen, R. Corke, N. Desai, P. Ilten, S. Mrenna, S. Prestel, C. O. Rasmussen, and P. Z. Skands, *An introduction to PYTHIA 8.2*, *Comput. Phys. Commun.* **191** (2015) 159–177, [[arXiv:1410.3012](#)].
- [80] M. Cacciari, G. P. Salam, and G. Soyez, *FastJet User Manual*, *Eur. Phys. J. C* **72** (2012) 1896, [[arXiv:1111.6097](#)].
- [81] DELPHES 3 Collaboration, J. de Favereau, C. Delaere, P. Demin, A. Giammanco, V. Lemaitre, A. Mertens, and M. Selvaggi, *DELPHES 3, A modular framework for fast simulation of a generic collider experiment*, *JHEP* **02** (2014) 057, [[arXiv:1307.6346](#)].
- [82] A. J. Larkoski, G. P. Salam, and J. Thaler, *Energy Correlation Functions for Jet Substructure*, *JHEP* **06** (2013) 108, [[arXiv:1305.0007](#)].
- [83] T. Chen and C. Guestrin, *XGBoost: A Scalable Tree Boosting System*, *CoRR* (2016) [[arXiv:1603.02754](#)].

- [84] A. L. Read, *Presentation of search results: The CL(s) technique*, *J. Phys. G* **28** (2002) 2693–2704.
- [85] G. Cowan, K. Cranmer, E. Gross, and O. Vitells, *Asymptotic formulae for likelihood-based tests of new physics*, *Eur. Phys. J. C* **71** (2011) 1554, [[arXiv:1007.1727](#)]. [Erratum: *Eur.Phys.J.C* **73**, 2501 (2013)].
- [86] L. Heinrich, M. Feickert, and G. Stark, *pyhf: v0.6.2*, .
<https://github.com/scikit-hep/pyhf/releases/tag/v0.6.2>.
- [87] L. Heinrich, M. Feickert, G. Stark, and K. Cranmer, *pyhf: pure-python implementation of histfactory statistical models*, *Journal of Open Source Software* **6** (2021), no. 58 2823.
- [88] J. Fuentes-Martin, G. Isidori, J. Pagès, and B. A. Stefanek, *Flavor non-universal Pati-Salam unification and neutrino masses*, *Phys. Lett. B* **820** (2021) 136484, [[arXiv:2012.10492](#)].
- [89] L. Allwicher, G. Isidori, and A. E. Thomsen, *Stability of the Higgs Sector in a Flavor-Inspired Multi-Scale Model*, *JHEP* **01** (2021) 191, [[arXiv:2011.01946](#)].